NAVAL POSTGRADUATE SCHOOL

MONTEREY, CALIFORNIA

THESIS

AN ANALYSIS OF THREE-CHANNEL RSNS VIRTUAL SPACING DIRECTION FINDING SYSTEM

by

Kevin Kwai

December 2007

Thesis Advisors: Phillip Pace
David Jenn
Donald Walters

Approved for public release; distribution is unlimited

THIS PAGE INTENTIONALLY LEFT BLANK

REPORT DOCUMENTATION PAGE		*Form Approved OMB No. 0704-0188*

Public reporting burden for this collection of information is estimated to average 1 hour per response, including the time for reviewing instruction, searching existing data sources, gathering and maintaining the data needed, and completing and reviewing the collection of information. Send comments regarding this burden estimate or any other aspect of this collection of information, including suggestions for reducing this burden, to Washington headquarters Services, Directorate for Information Operations and Reports, 1215 Jefferson Davis Highway, Suite 1204, Arlington, VA 22202-4302, and to the Office of Management and Budget, Paperwork Reduction Project (0704-0188) Washington DC 20503.

1. AGENCY USE ONLY *(Leave blank)*	2. REPORT DATE December 2007	3. REPORT TYPE AND DATES COVERED Master's Thesis	
4. TITLE AND SUBTITLE An Analysis of Three-Channel RSNS Virtual Spacing Direction Finding System		**5. FUNDING NUMBERS**	
6. AUTHOR(S) Kevin Kwai			
7. PERFORMING ORGANIZATION NAME(S) AND ADDRESS(ES) Naval Postgraduate School Monterey, CA 93943-5000		**8. PERFORMING ORGANIZATION REPORT NUMBER**	
9. SPONSORING /MONITORING AGENCY NAME(S) AND ADDRESS(ES) N/A		**10. SPONSORING/MONITORING AGENCY REPORT NUMBER**	
11. SUPPLEMENTARY NOTES The views expressed in this thesis are those of the author and do not reflect the official policy or position of the Department of Defense or the U.S. Government.			
12a. DISTRIBUTION / AVAILABILITY STATEMENT Approved for public release; distribution is unlimited		**12b. DISTRIBUTION CODE**	

13. ABSTRACT (maximum 200 words)

The design and performance analysis of a three-channel Robust Symmetrical Number System (RSNS) virtual spacing direction finding (DF) system was carried out in this thesis. The design was based on hardware used in the previous work in which a digital three-channel RSNS-based interferometer was built. In designing a RSNS virtual spacing DF system, it was found that the ratio between the modulus is an important parameter. The ratio affects the selection of the moduli set, the array size and the system's field of view. Based on the hardware used, the system's signal-to-noise ratio (SNR) was determined for a simulated emitter. Random Gaussian noise was injected into the system to determine the accuracy of mapping the actual angle-of-arrival (AOA) to the estimated AOA. Monte Carlo simulations were carried out to determine the probability of correctly estimating the AOA of the signal. Simulation results from the effect of spacing errors, phase errors, frequency error, moduli set change and SNR change was presented and analyzed. The RSNS-based DF system was found to be relatively insensitive to spacing error. A proposed two set of moduli were used to improve the accuracy and probability of correct estimation in both low SNR and high SNR conditions.

14. SUBJECT TERMS Direction Finding, Robust Symmetrical Number System, Variable Resolution, Additive Gaussian Noise			**15. NUMBER OF PAGES** 91
			16. PRICE CODE
17. SECURITY CLASSIFICATION OF REPORT Unclassified	**18. SECURITY CLASSIFICATION OF THIS PAGE** Unclassified	**19. SECURITY CLASSIFICATION OF ABSTRACT** Unclassified	**20. LIMITATION OF ABSTRACT** UU

Standard Form 298 (Rev. 8-98)
Prescribed by ANSI Std. Z39.18

THIS PAGE INTENTIONALLY LEFT BLANK

AN ANALYSIS OF THREE-CHANNEL RSNS VIRTUAL SPACING DIRECTION FINDING SYSTEM

Kevin Kwai Kiah Wen
Major, Republic of Singapore Airforce
B.Eng., University of Manchester Institute of Science and Technology, 1999

Submitted in partial fulfillment of the
requirements for the degree of

MASTER OF SCIENCE IN COMBAT SYSTEMS SCIENCE AND TECHNOLOGY

from the

**NAVAL POSTGRADUATE SCHOOL
December 2007**

Author: Kevin Kwai

Approved by: Phillip E. Pace
                 Thesis Advisor

                 David C. Jenn
                 Thesis Advisor

                 Donald L. Walters
                 Thesis Advisor

                 James H. Luscombe
                 Chairman, Department of Physics

THIS PAGE INTENTIONALLY LEFT BLANK

ABSTRACT

The design and performance analysis of a three-channel Robust Symmetrical Number System (RSNS) virtual spacing direction finding (DF) system was carried out in this thesis. The design was based on hardware used in the previous work in which a digital three-channel RSNS-based interferometer was built. In designing a RSNS virtual spacing DF system, it was found that the ratio between the modulus is an important parameter. The ratio affects the selection of the moduli set, the array size and the system's field of view. Based on the hardware used, the system's signal-to-noise ratio (SNR) was determined for a simulated emitter. Random Gaussian noise was injected into the system to determine the accuracy of mapping the actual angle-of-arrival (AOA) to the estimated AOA. Monte Carlo simulations were carried out to determine the probability of correctly estimating the AOA of the signal. Simulation results from the effect of spacing errors, phase errors, frequency error, moduli set change and SNR change was presented and analyzed. The RSNS-based DF system was found to be relatively insensitive to spacing error. A proposed two set of moduli were used to improve the accuracy and probability of correct estimation in both low SNR and high SNR conditions.

THIS PAGE INTENTIONALLY LEFT BLANK

TABLE OF CONTENTS

LIST OF FIGURES

LIST OF TABLES

THIS PAGE INTENTIONALLY LEFT BLANK

ACKNOWLEDGMENTS

I would like to thank my thesis advisors, Professor Phillip E. Pace, Professor David C. Jenn and Professor Donald Walters, for their guidance, patience and understanding throughout my thesis project. To begin to do research into an area unfamiliar to me was never going to be an easy task. They have provided me with guidance as well as invaluable insight.

I would like to thank the Republic of Singapore Airforce for the opportunity to do my Master's at the Naval Postgraduate School.

I would like to thank my wife Jo for her understanding and support during my stay at NPS. With her along my side, nothing seems insurmountable, and she will always be my perfect companion in my journey through life. Last but not least, I would like to dedicate this thesis to Lucas and Vivien, my wonderful twins, who have given me a direction in life that just makes everything so clear.

THIS PAGE INTENTIONALLY LEFT BLANK

I. INTRODUCTION

A. DIRECTION FINDING

Radio direction finding is a class of direction finding (DF) by which the direction to a microwave signal is determined by means of a radio direction finder (RDF). A RDF is a receiving system that analyzes the information extracted from the passing electromagnetic radio wave to obtain direction of arrival (DOA) information [1]. In military context, some of the more important uses of direction finding relating to electronic warfare applications include early warning threat detection, targeting and electronic intelligence [2].

An RDF could be separated into three broad categories depending on the method by which it determined the angle of arrival (AOA) of the signal. The three categories are [2]:

1. Amplitude Comparison

2. Phase Delay

3. Time Delay

Amplitude Comparison uses either a direct or comparative method to obtain AOA information from the amplitude response of the antenna elements.

Phase Delay and Time Delay systems extract the AOA information by a similar principle except that the former used phase information while the latter used the time of arrival information of the wave. Both systems required at least two separate antennas with pre-determined spacing. Figure 1 showed how a phase delay or time delay method would work. The plane wave would arrive at antenna element 1 earlier than antenna element 2. The antenna spacing, d, would cause a time delay or phase delay between the antenna elements. Assuming that the frequency of the wave and the antenna spacing are known, the AOA can be determined.
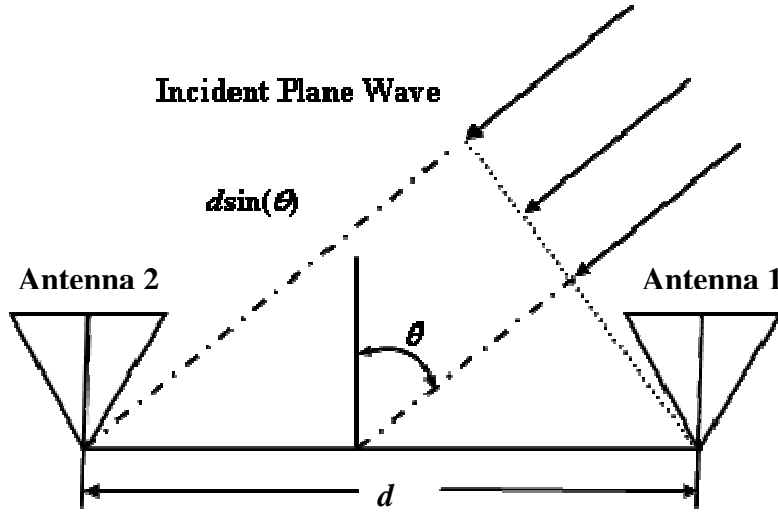
Figure 1.   Basic phase-delay / time-delay interferometry (After [1]).

To increase resolution, a larger antenna spacing is usually used. However, a larger antenna spacing also introduces ambiguities. If the spacing is greater than a half-wavelength distance, more than one unique AOA exists.

B.   PREVIOUS WORK

Through the years, research into using a Robust Symmetrical Number System (RSNS) for direction finding has been investigated in order to achieve high resolution with a small antenna baseline. It has been shown that a three-channel DF array based on RSNS theory and using a digital architecture can achieve a good resolution of 1.25 degrees RMS with a baseline of 66.2 cm [3].

C.   PRINCIPAL CONTRIBUTIONS

This thesis focused on the design and analysis of a three-channel virtual spacing DF system with two levels of processing. Design considerations for the

RSNS virtual spacing DF system was analyzed. It highlighted the importance of selecting the appropriate modulus ratio for sizing of the antenna array as well as field of view requirements.

By analyzing the hardware used in the previous implementation of the RSNS-based DF system, the receiver's noise figure was determined. From the noise figure, a link equation was used to calculate the theoretical signal-to-noise ratio (SNR) of a simulated emitter. Simulations were carried out using this link equation in determining the performance of a three-channel RSNS virtual spacing DF system. The effects of spacing errors, phase errors, frequency errors, moduli set change and SNR change were determined from the results of the simulation. Monte Carlo simulations were carried out to determine the probability of correctly estimating the AOA of the signal. Simulation results from the effect of spacing errors, phase errors, frequency error, moduli set change and SNR change was presented and analyzed. The RSNS-based DF system was found to be relatively insensitive to spacing error. A proposed two set of moduli were used to improve the accuracy and probability of correct estimation in both low SNR and high SNR conditions.

D. THESIS OUTLINE

Chapter II reviews the basic operating principles of RDF systems and provides the fundamental basis for applying the RSNS for direction finding.

Chapter III introduces the RSNS theory and how it can be applied to phase interferometry. Previous experimental results are also presented.

Chapter IV explains how the RSNS interferometry works with virtual resolution.

Chapter V presents the considerations for designing a three-channel RSNS virtual spacing direction finding system.

Chapter VI explains the models used in the simulation.

Chapter VII presents the results and analysis of the simulations.

Chapter VIII presents the conclusion.

THIS PAGE INTENTIONALLY LEFT BLANK

II. PHASE DELAYED-BASED INTERFEROMETRY

This chapter reviews the basic operating principle of phase delayed-based interferometry and how AOA ambiguities can arise.

A. THEORY

It is assumed that the DF array operates in the far field; hence the incident electromagnetic wave is planar. A one-channel linear interferometer is shown in Figure 2. The two antenna elements are space a distance d apart and the incident plane wave arrives at an angle θ as shown. The angle of arrival can vary over a range of $\pm 90°$.
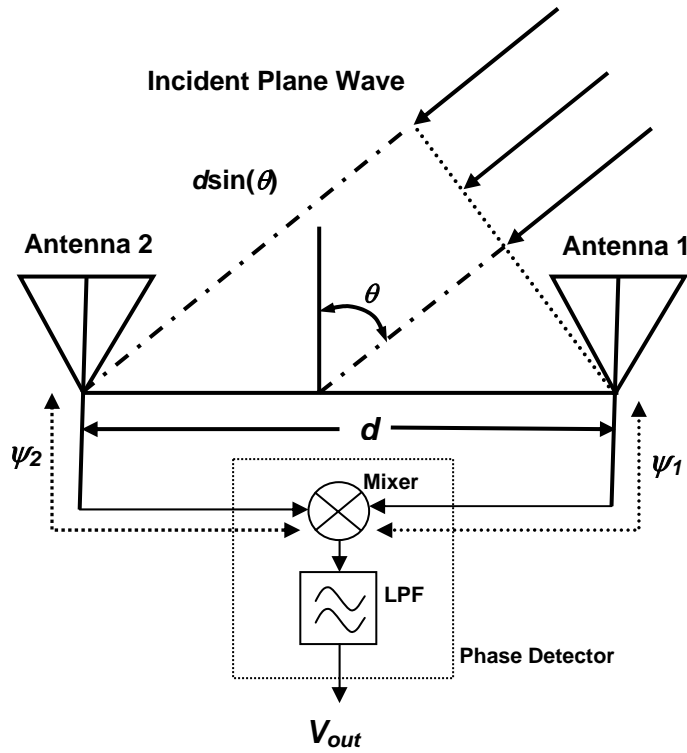
Figure 2.   Two-element interferometry (From [4]).

The incident wave arrives at antenna element 1 first and after an additional distance of $d \sin(\theta)$, it arrives at antenna element 2. A sinusoidal (time-harmonic) signal received by the antenna elements has the following form:

$$V_i = V \cos(\omega_c t + \psi_i + \phi_i) \tag{2.1}$$

where i denotes the element index number; V is the signal amplitude response, ω_c is the signal frequency in radians/sec, ψ_i is the phase term due to the cables and ϕ_i is the phase term due to path delay relative to the reference antenna (antenna 1). The received signals are fed into an analog phase detector which consists of a mixer and a low-pass filter (LPF). After the phase detection mixing process, the output voltage has the following form:

$$V_{mix}(\phi,t) = V_1(\phi_1,t)V_2(\phi_2,t) = \frac{V^2}{2}\left[\cos(2\omega_c t + \sum \psi + \sum \phi) + \cos(\Delta \psi + \Delta \phi)\right] \tag{2.2}$$

The term $\Delta \psi$ results from the phase differential due to cable length differences. The term $\Delta \phi$ results from the phase differential due to the additional $d \sin(\theta)$ distance traveled by the signal wave-front to reach antenna element 2 and it can be written as

$$\Delta \phi = \phi_1 - \phi_2 = kd \sin(\theta) \tag{2.3}$$

where $k = \frac{2\pi}{\lambda}$ and λ is the wavelength.

After the LPF removes the high frequency component of the signal, the output signal which remains is

$$V_{out}(\phi) = \frac{V^2}{2}\cos(\Delta \psi + \Delta \phi) \tag{2.4}$$

We can measure $\Delta \psi$ and eliminate it. After normalizing the voltage's amplitude, the final output signal is

$$V_{out}(\phi) = \cos(\Delta \phi) = \cos(kd \sin(\theta)) \tag{2.5}$$

B.   AMBIGUITY

As the phase differential term repeats itself with a period of 2π, it can result in an ambiguity if distance between the antenna elements is greater than half a wavelength. To illustrate this point, we first consider a case where $d = \lambda/2$, which gives $\Delta\phi = \pi\sin(\theta)$. There will be a one-to-one mapping of the AOA to the phase difference as shown in Figure 3 and no ambiguity exists.
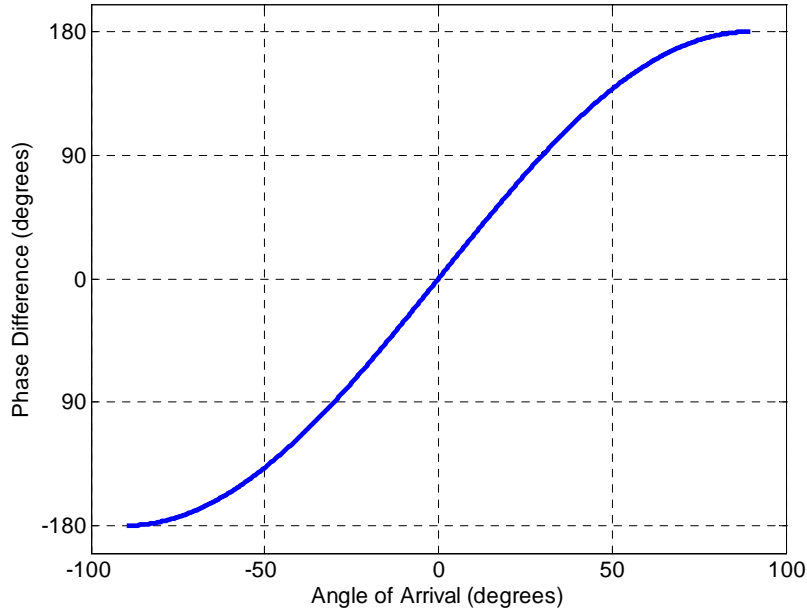
Figure 3.   Phase differential vs AOA for $d = \lambda/2$ (From [5]).

Next, we consider a case where $d = \lambda$, which gives $\Delta\phi = 2\pi\sin(\theta)$. For every phase difference measured, there will be two possible AOAs as shown in Figure 4.
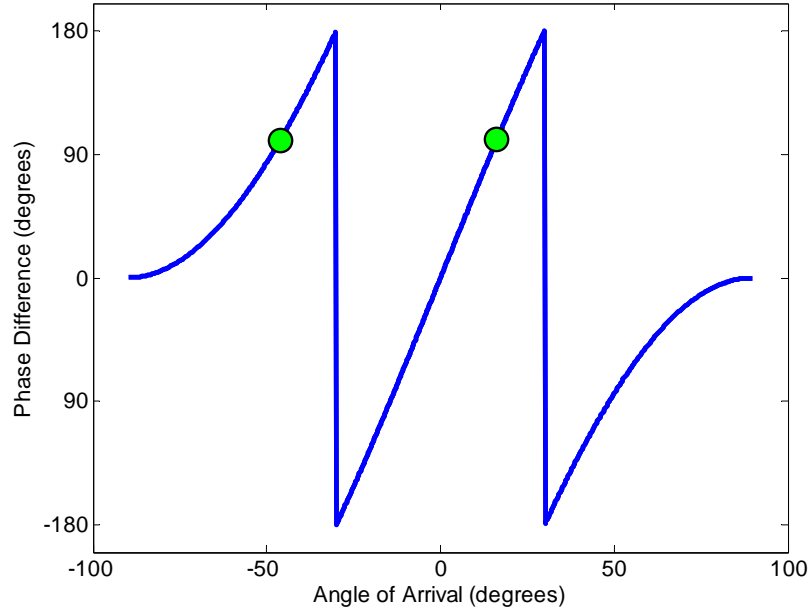
Figure 4. Phase differential vs AOA for $d=\lambda$ (From [6]).

The accuracy of the AOA measurement can be stated as the change in phase difference for a given change in AOA. Hence from Equation (2.4),

$$\frac{\partial(\Delta\phi)}{\partial\theta} = kd\cos(\theta) \tag{2.6}$$

For any given frequency and AOA, Equation (2.6) shows that the accuracy of the measurement is directly proportional to the distance d. Hence, a longer baseline would give a more accurate measurement.

To overcome the ambiguity coupled with the need for higher angular resolution, dual baselines are often used. The longer baseline is used to provide the high angular resolution required, while the shorter baseline is used to resolve any ambiguities [2].

C. FOLDING WAVEFORMS

The output voltage from any two antenna elements can be represented by Equation (2.5). For the cases of $d = \dfrac{\lambda}{2}$ and $d = \lambda$, the normalized voltages are

8

plotted in Figure 5. It shows that the both waveforms are symmetrical about the zero angle of arrival (broadside) and the visible region is from ±90 degrees. The number of folding periods, *n*, within the visible region is given by

$$n = \frac{d}{\lambda/2} = \frac{2d}{\lambda}$$

(2.7)
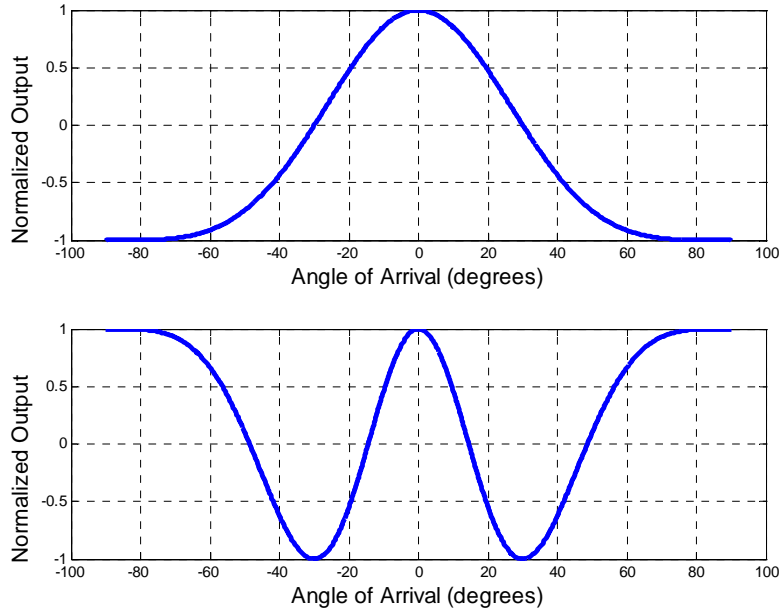
Figure 5. Output voltage vs AOA for $d = \lambda/2$ and $d = \lambda$ (From [3]).

In a binary interferometer system where each successive baseline is changed by a factor of two, it is possible to resolve an ambiguity of the longer baseline and yet achieve higher resolution [2]. A three-channel interferometer is shown in Figure 6. The successive baseline is changed by the factor of 2.

9
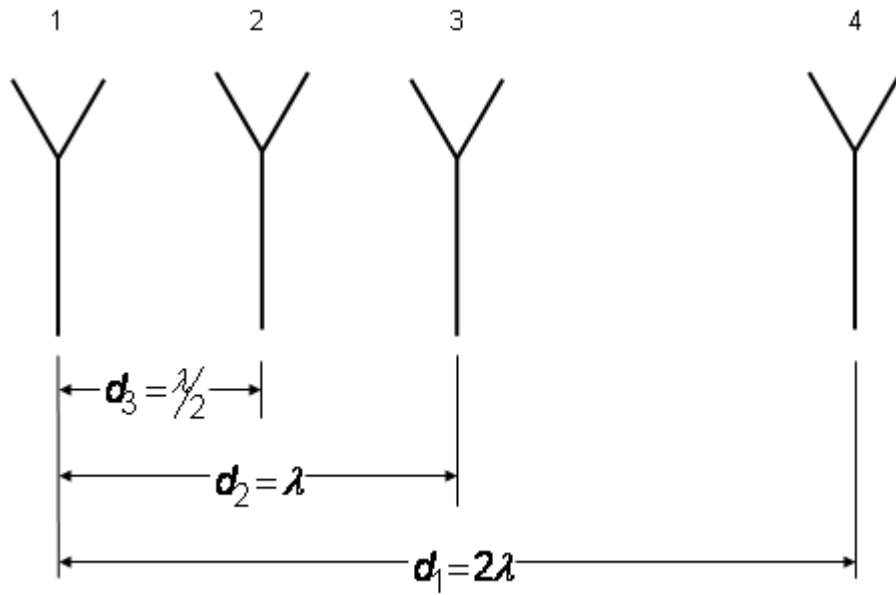
Figure 6.   Three-channel interferometer with binary relationship
between spacing (From [2]).

The size of the physical antenna element array is often the limitation in determining the accuracy of the DF system. The next chapter introduces another method of increasing resolution without the requirement of a larger antenna element baseline.

III. ROBUST SYMMETRICAL NUMBER SYSTEM-BASED DIRECTION FINDING

As it is advantageous to have a higher resolution without the need for a large antenna baseline, a signal preprocessing method utilizing the robust symmetrical number system (RSNS) was introduced to DF in [3-7]. This chapter reviews the RSNS theory and how it is implemented in phase interferometry.

A. THE ROBUST SYMMETRICAL NUMBER SYSTEM

The main idea behind RSNS-based direction finding is to represent a symmetrical waveform out of an antenna by a RSNS sequence. The RSNS is based on a sequence defined as

$$x_m = [0,1,2,....,m-1,m,m+1,....,2,1] \tag{3.1}$$

where x_m is a row vector and m is the modulus and is a positive integer ($m>0$).

In an N-channel RSNS [8], where $N \geq 2$, the basic sequence for the ith channel with modulus m is

$$x_{mi} = [0_0,0_1,....,0_N,1_0,1_1,....,1_N,....,m_0,m_1,....,m_N,....,1_0,1_1,....,1_N] \tag{3.2}$$

The sequence is repeated in both directions and it forms a sequence with a period of

$$P_{RSNS} = 2Nm_i \tag{3.3}$$

Considering a single channel, the discrete states of the RSNS can be expressed as

$$g = \begin{cases} \left\lfloor \left| \dfrac{n-s_i}{N} \right| \right\rfloor & s_i \leq n \leq Nm_i + s_i + 1 \\[3ex] \left\lfloor \left| \dfrac{2Nm_i + N - n + s_i - 1}{N} \right| \right\rfloor & Nm_i + s_i + 2 \leq n \leq 2Nm_i + s_i - 1 \end{cases} \tag{3.4}$$

where

11

g is the nth level of channel I,

m_i is the ith channel modulus,

s_i is the corresponding sequence shift $s_i \equiv 0,1,2,....,N-1$ (mod N) and $N \geq 2$ is the number of sequences in the system.

The values $(s_1, s_2, ..., s_N)$ must form a complete residue system modulo N and because of the relative property of the shifts, one of the shift values will be set equal to 0.

An N-channel RSNS is formed by selecting N moduli and N shift values s_i, $(1 \leq i \leq N)$. Since the fundamental period for channel i is $2Nm_i$, the RSNS vectors must be a mutilple of $2Nm_i$. Hence, the fundamental period for the RSNS is

$$PF_{RSNS} = \{2m_1N, 2m_2N, ..., 2m_NN\} \tag{3.5}$$

where $\{a_1, a_2, ..., a_N\}$ is the least common multiple of $a_1, a_2, ..., a_N$. From Equation (3.5),

$$PF_{RSNS} = 2N\{m_1, m_2, ..., m_N\} \tag{3.6}$$

To illustrate the RSNS, consider a modulus set of $\begin{bmatrix} 3 & 4 \end{bmatrix}$ where $m_1 = 3(s_1 = 0)$ and $m_2 = 4(s_2 = 1)$. Table 1 shows the sequences illustrating the inherent integer Gray-code property.

I	0	1	2	3	4	5	6	7	8	9	10	11	12	13	14	15	16	17	18	19
$m_1 = 3$	0	1	1	2	2	3	3	2	2	1	1	0	0	1	1	2	2	3	3	2
$m_2 = 4$	0	0	1	1	2	2	3	3	4	4	3	3	2	2	1	1	0	0	1	1
n					0	1	2	3	4	5	6	7	8	9	10	11	12	13	14	

Table 1. RSNS sequence for $m_1 = 3(s_1 = 0)$ and $m_2 = 4(s_2 = 1)$
(From [6]).

The system dynamic range, $\hat{M}$, is the maximum number of distinct vectors without any ambiguity. From Table 1, the dynamic range for $[3\ 4]$ is $\hat{M}$=15. It was shown that the shifts employed will affect the dynamic range sequence starting and ending points but it does not have any effect on the value of $\hat{M}$ [9].

The dynamic range of several moduli in combination has been formulated in closed form [10]. For two channels, there are three cases of two relatively prime moduli m_1 and m_2 that yield $\hat{M}$.

- Case I: For $m_1 \geq 3$ and $m_2 = m_1 + 1$,

$$\hat{M} = 3(m_1 + m_2) - 6 \tag{3.7}$$

- Case II: For $m_1 \geq 5$ and $m_2 = m_1 + 2$,

$$\hat{M} = 3(m_1 + m_2) - 7 \tag{3.8}$$

- Case III: For $m_1 \geq 5$ and $m_2 = m_1 + C$, and $C \geq 3$,

$$\hat{M} = 4m_1 + 2m_2 - 2 \tag{3.9}$$

For the example in Table 1, which satisfies Equation (3.7),

$$\hat{M} = 3(m_1 + m_2) - 6 = 3(3 + 4) - 6 = 15.$$

For three channels, there are two cases of closed form solution that have been formulated [11, 12].

- Case I: For $m_1 = 2^k - 1$, $m_2 = 2^k + 1$ for $m_1 \geq 3$,

$$\hat{M} = \frac{3}{2}m_1^2 + \frac{15}{2}m_1 + 7 \tag{3.10}$$

- Case II: For $m_1 = 2m_2 + 1$, $m_3 = 4m_1 + 1$,

$$\hat{M} = 6m_1^2 + 21m_1 + 3 \tag{3.11}$$

As the closed form solution covers only limited cases, it has been shown that the most efficient method of determining the dynamic range is by using a search algorithm [12, 13].

B.   THE RSNS INTERFEROMETER DESIGN

The design of an RSNS interferometer has been simplified into eight steps by Lee in his Master's thesis [3]. The eight steps are:

1.   **Determine *N*, the number of channels required.**

2.   **Identify an integer valued modulus for each channel ($m_1 \dots m_N$).**

3.   **Determine the system dynamic range, $\hat{M}$, based on the chosen moduli.**

4.   **Determine the number of folds, n_i, for each modulus.**

The number of folds is determined by

$$n_i = \frac{\hat{M}}{P_{RSNS}} = \frac{\hat{M}}{2Nm_i} \qquad (3.12)$$

5.   **Determine the required antenna spacing, d_i, for each channel.**

$$d_i = n_i \frac{\lambda}{2} = \frac{\hat{M}\lambda}{4Nm_i} \qquad (3.13)$$

6.   **Re-mapping the Field of View (FOV).**

This is an optional step. The gain of an antenna reduces as the AOA increases from the broadside and to get a high signal-to-noise ratio (SNR) for digital processing, the FOV can be compressed into a suitable range. This increases resolution and decreases the antenna spacing required [4]. By keeping *k* and V_{out} constant in Equation (2.5), we get

$$d\sin(\theta_{max}) = d'\sin(\theta'_{max}) \qquad (3.14)$$

where θ_{max} is the maximum FOV and *d* is the antenna spacing of the original configuration. The quantities θ'_{max} and *d'* are the maximum FOV and antenna spacing for the scaled configuration. The scale factor, ξ, is defined as

$$\xi = \frac{d'}{d} = \frac{\sin(\theta_{max})}{\sin(\theta'_{max})} \tag{3.15}$$

Combining Equation (3.13) and Equation (3.15), the scaled antenna spacing can be determined.

$$d'_{max} = d_i \xi = \frac{\hat{M}\lambda}{4m_i N} \xi \tag{3.16}$$

7.   Determine the thresholds.

For a digital architecture, the thresholds to amplitude analyze the folding phase waveform into the RSNS. It has been shown [4] that for a normalized folding waveform, the threshold for the jth comparator of modulus channel m_i can be determine by

$$V_{j,m_i} = \cos\left(\frac{m_i - j + \frac{1}{2}}{m_i}\pi\right), \qquad 1 \le j \le m_i. \tag{3.17}$$

When the waveform exceeds a threshold, it will be encoded to the next integer value. Figure 7 shows how the folding waveform in Table 1 can be encoded by Equation (3.17). At the boxed in section of $\hat{M}$, the symmetrical residues are $s_1 = 0$ $(m_1 = 3)$ and $s_2 = 3$ $(m_2 = 4)$.

15
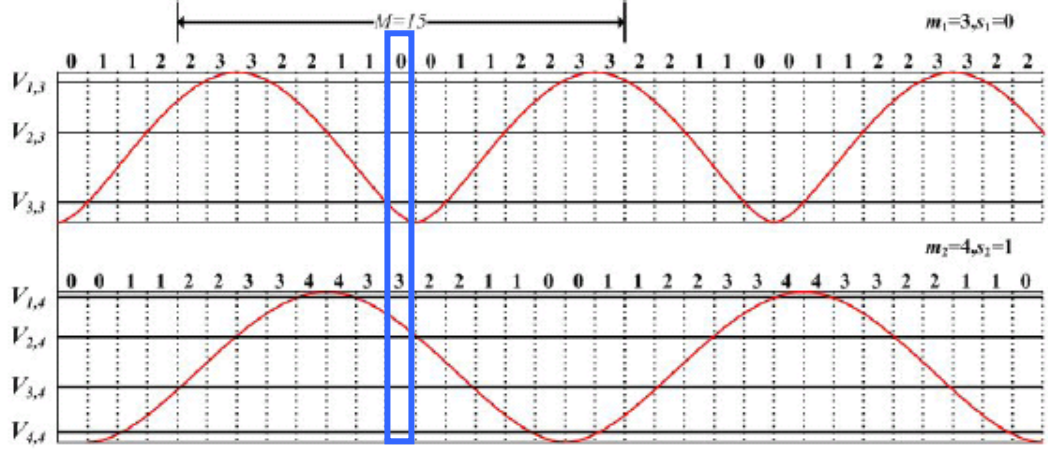
Figure 7.   Mapping RSNS folding waveforms to threshold values (From [5]).

8.   **Calculate the phase adjustment term, ζ , for each channel.**

From Figure 7, both moduli do not have symmetry about the center of the dynamic range at $n=7$. A phase adjustment term, ζ , is thus required to shift the center of the dynamic range to the signal AOA at the broadside. From Equation (2.5), the phase adjustment term is added:

$$V_{out}(\theta) = \cos\left(kd\sin\theta + \zeta\right) \tag{3.18}$$

The relationship between the RSNS coding and the AOA has been obtained at this point. Using this relationship, a transfer function of the estimated AOA against the true AOA can be plotted. Previous studies have shown that the estimated AOA, θ'_u, for the uth bin is given as [4]:

$$\theta'_u = \sin^{-1}\left(\frac{2u+1}{\hat{M}\xi} - \frac{1}{\xi}\right) \tag{3.19}$$

and the resolution, r_u, for the uth bin is given by:

$$r_u = \sin^{-1}\left(\frac{2u - \hat{M} + 2}{\hat{M}\xi}\right) - \sin^{-1}\left(\frac{2u - \hat{M}}{\hat{M}\xi}\right) \tag{3.20}$$

16

C.   DESIGN EXAMPLE

A three-channel RSNS DF system was designed and implemented by Lee in his master's thesis [3]. Using the eight steps as previously described, his design is used as an example to explain how these steps are carried out in detail.

1.   Determine *N*, the number of channels required.

It was decided a three channel DF system was to be designed. Hence, $N=3$ and a total of four antenna elements would be required.

2.   Identify an integer valued modulus for each channel ($m_1…m_N$).

The moduli set of [7 15 29] was chosen for high resolution as well as a relatively short antenna baseline. It is important to note that there will be other viable alternatives to the moduli set and the current set was chosen because it consists of pairwise relatively prime (PRP) numbers.

3.   Determine the system dynamic range, $\hat{M}$, based on the chosen moduli.

Using a MATLAB search program, the dynamic range for the moduli set was found to be $\hat{M} = 444$.

4.   Determine the number of folds, n_i, for each modulus.

Applying Equation (3.12), the number of folds for each channel sequence was found to be,

$$n_1 = \frac{\hat{M}}{2Nm_1} = \frac{444}{2(3)(7)} = 10.57$$

$$n_2 = \frac{\hat{M}}{2Nm_2} = \frac{444}{2(3)(15)} = 4.93$$

$$n_3 = \frac{\hat{M}}{2Nm_1} = \frac{444}{2(3)(29)} = 2.55$$

5.   Determine the required antenna spacing, d_i, for each channel.

At this step, it was decided that a signal frequency of 2.4 GHz be selected as there were readily available component hardware in the laboratory, which could be used for building the array. For a signal of 2.4 GHz, the wavelength, λ, is 12.5 cm.   Applying Equation (3.13), the distances between pairs of antenna elements are,

$$d_1 = n_1 \frac{\lambda}{2} = 10.57 \left(\frac{12.5}{2} \right) = 66.07 \text{ cm}$$

$$d_2 = n_2 \frac{\lambda}{2} = 4.93 \left(\frac{12.5}{2} \right) = 30.83 \text{ cm}$$

$$d_3 = n_3 \frac{\lambda}{2} = 4.93 \left(\frac{12.5}{2} \right) = 15.95 \text{ cm}.$$

6.   Re-mapping the Field of View (FOV).

The FOV was not scaled and hence the scaled factor $\xi = 1 \left(\pm 90° \right)$.

7.   Determine the thresholds.

Each channel would have a number of thresholds corresponding to the chosen modulus number.   For a modulus of 7, there would be 7 thresholds. Similarly, modulus of 15 and 29 would have 15 and 29 thresholds respectively. The threshold levels for the chosen moduli [7 15 29] are shown graphically in Figure 8 below using Equation (3.17).
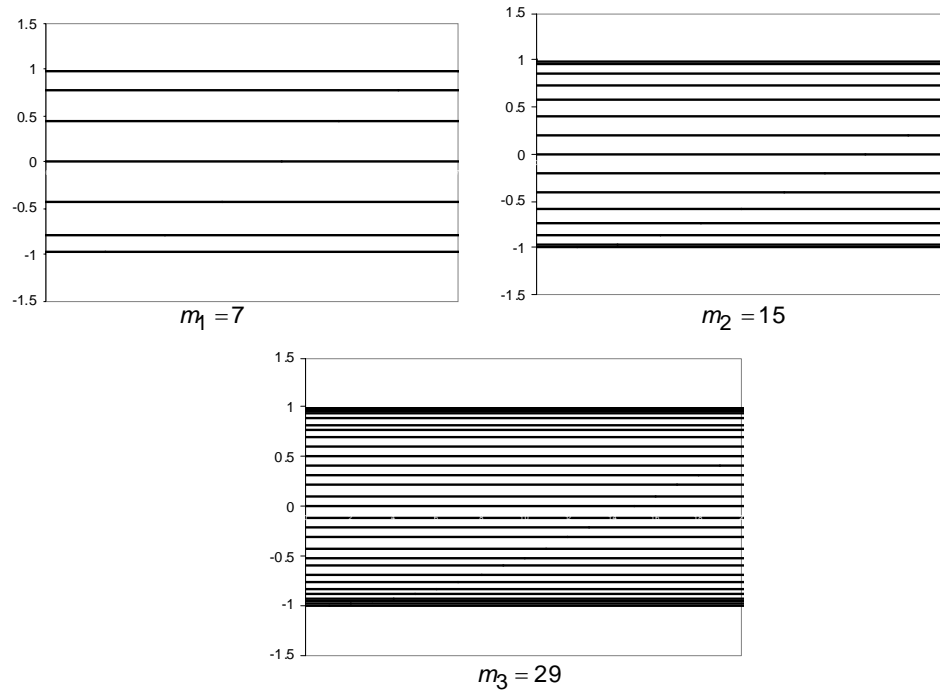
Figure 8.   Threshold levels for moduli set [7 15 29].

8.   Calculate the phase adjustment term, ζ , for each channel.

The phase adjustment terms, ζ_i, were similarly found by a MATLAB search program. The phase adjustment terms are shown in Table 2.

	Phase Adjustment Term
Channel 1, ζ_1	-1.4960 radians
Channel 2, ζ_2	0.0698 radians
Channel 3, ζ_3	0.8666 radians

Table 2.   Phase adjustment term for moduli set [7 15 29] (From [3]).

D. SIMULATION RESULTS

Using Equation (3.18), the folding waveforms for all the channels were plotted in Figure 9. The corresponding encoded waveforms were also plotted in Figure 10. By using Equation (3.19), the estimated AOA can be plotted against the true AOA as shown in Figure 11.
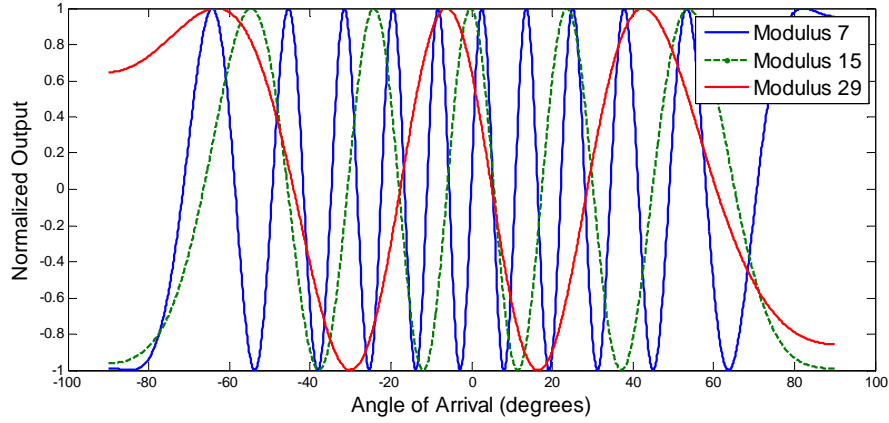
Figure 9.   Folding waveforms with phase adjustment.
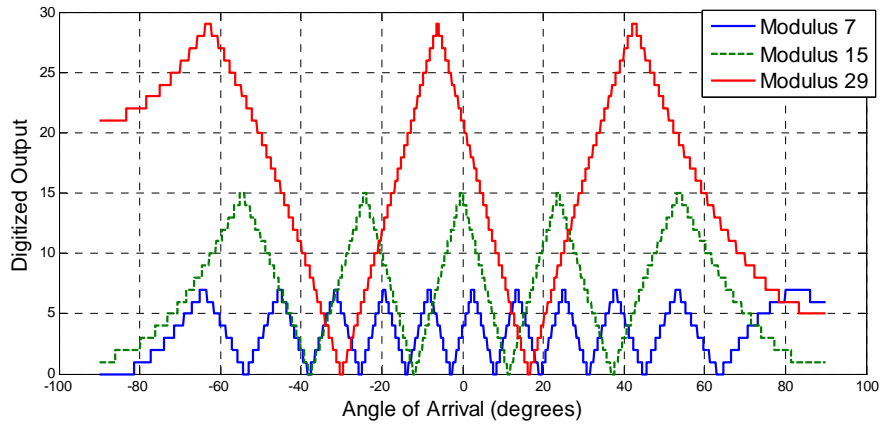
Figure 10.   Phase adjusted folding waveforms after encoding.
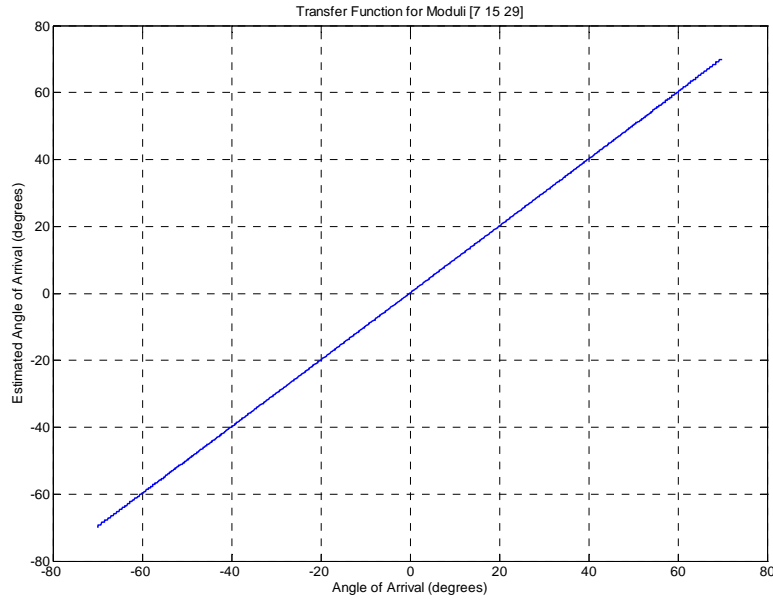
Figure 11.   Transfer function for demonstration array using
moduli [7 15 29] (From [3]).

E.   EXPERIMENTAL RESULTS

A RSNS-based DF array was built and tested using same design as described in Section D. The experimental results are shown in Figure 12. The experimental results showed that although there are errors appearing intermittently throughout the AOA, the basic feature of the transfer function remains similar to the ideal transfer function as shown in Figure 11. The errors are likely due to antenna spacing error and phase errors from the demodulator boards [3].
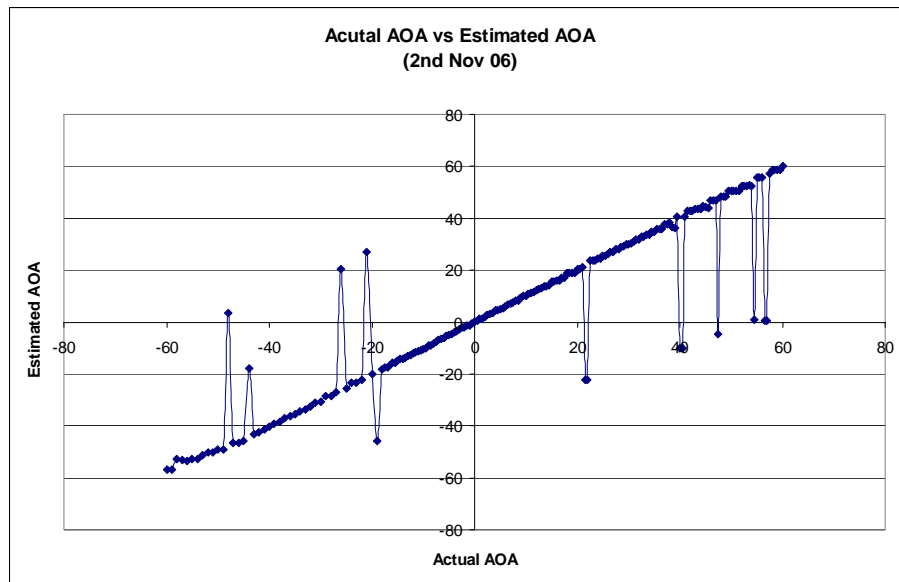
Figure 12.   Experimental results for demonstration array
using moduli [7 15 29] (From [3]).

IV. RSNS INTERFEROMETRY WITH VIRTUAL SPACING

Virtual spacing for RSNS interferomery was first proposed by Chen for a two-channel system and it was later extended to an *N*-channel system by Lee [3, 6]. This chapter introduced how quadrature demodulation works followed by an explanation of how a two-channel interferometer works. Finally, a three-channel virtual spacing DF system is presented.

A. QUADRATURE DEMODULATION

The bandpass signal can be expressed by the in-phase component and the qaudrature component as

$$x_{band}(t) = x_I \cos(\omega_c t) - x_Q \sin(\omega_c t) \qquad (4.1)$$

where x_I is the in-phase component,

x_Q is the quadrature component, and

$\omega_c = 2\pi f_c$, f_c is the carrier frequency.
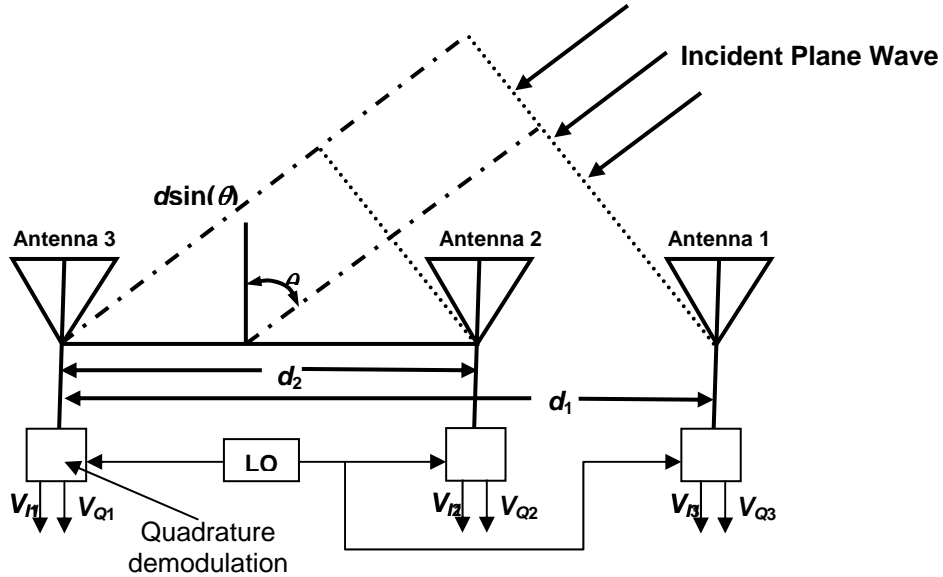
Figure 13.   Quadrature type demodulation of two-channel interferometer
(From [3]).

23

The output voltage from the antenna elements as shown in Figure 13 can be expressed as

$$V(p_n,t) = \text{Re}\left(A(p_n)e^{j(\omega_c t)}\right) \tag{4.2}$$

where $n = 1,2,3$ is the antenna element index, p_n is the position at antenna element n, t is the time. $A(p_n)$ is defined as

$$A(p_n) = |A(p_n)|e^{j\phi(p_n)} = A_I(p_n) + jA_Q(p_n) \tag{4.3}$$

The output voltage can be mixed with a local oscillator signal to get the in-phase and quadrature terms

$$V_I(p_n,t) = V(p_n,t)\cos(\omega_c t)$$
$$= \frac{1}{2}A_I(p_n) + \frac{1}{2}[A_I(p_n)\cos(2\omega_c t) - A_Q(p_n)\sin(2\omega_c t)] \tag{4.4}$$

$$V_Q(p_n,t) = -V(p_n,t)\sin(\omega_c t)$$
$$= -\frac{1}{2}[A_I(p_n)\sin(2\omega_c t) + A_Q(p_n)\cos(2\omega_c t)] + \frac{1}{2}A_Q(p_n) \tag{4.5}$$

After low-pass filtering, the baseband terms that remain are

$$V_I(p_n) = \frac{1}{2}A_I(p_n) = \frac{1}{2}|A(p_n)|\cos(\phi(p_n)) \tag{4.6}$$

$$V_Q(p_n) = \frac{1}{2}A_Q(p_n) = \frac{1}{2}|A(p_n)|\sin(\phi(p_n)) \tag{4.7}$$

For a plane wave, let $|A(p_n)| = 1$. After normalizing Equations (4.6) and (4.7), the in-phase and quadrature terms of the received signals by antenna element n are

$$V_{In} = V_I(p_n) = \cos(\phi(p_n)) \tag{4.8}$$
$$V_{Qn} = V_Q(p_n) = \sin(\phi(p_n)) \tag{4.9}$$

The phase differential term between antenna element two and three can be found by

$$\Delta\phi_{23} = \phi(p_2) - \phi(p_3)$$
$$= \arctan\left(\frac{V_{Q2}}{V_{I2}}\right) - \arctan\left(\frac{V_{Q3}}{V_{I3}}\right) \tag{4.10}$$
$$= kd_2\sin\theta$$

Similarly, the phase differential term can be found for any other antenna pair. The in-phase and quadrature outputs for any channel using antenna element r as the reference, can be defined as

$$
\begin{aligned}
V_{IN}(\theta) &= \cos(kd_N \sin\theta) = \cos(\Delta\phi_{rn}) \\
&= \cos(\phi(p_n))\cos(\phi(p_r)) + \sin(\phi(p_n))\sin(\phi(p_r)) \\
&= V_{In}V_{Ir} + V_{Qn}V_{Qr}
\end{aligned}
\tag{4.11}
$$

$$
\begin{aligned}
V_{QN}(\theta) &= \sin(kd_N \sin\theta) = \sin(\Delta\phi_{rn}) \\
&= \sin(\phi(p_n))\cos(\phi(p_r)) - \cos(\phi(p_n))\sin(\phi(p_r)) \\
&= V_{In}V_{Ir} - V_{Qn}V_{Qr}
\end{aligned}
\tag{4.12}
$$

The phase adjustment term, ζ_i, is required for channel i so as to map the center of the dynamic range to the broadside. From Equation (3.18), the voltage from channel i can be expressed as

$$
V_i(\theta) = \cos\left(kd_i \sin(\theta) + \zeta_i\right)
\tag{4.13}
$$

Rearranging Equation (4.13),

$$
V_N(\theta) = \cos\left(kd_i \sin(\theta)\right)\cos(\zeta_i) - \sin\left(kd_i \sin(\theta)\right)\sin(\zeta_i)
\tag{4.14}
$$

$$
V_i(\theta) = V_{Ii}(\theta)\cos(\zeta_i) - V_{Qi}(\theta)\sin(\zeta_i)
\tag{4.15}
$$

B.   TWO-CHANNEL VIRTUAL SPACING INTERFEROMETRY

For a two-channel RSNS interferometer as shown in Figure 13, the moduli pair m_1 and m_2 is chosen. The dynamic range of the pair is $\hat{M}$. By combining the terms as given in Equation (4.12) and Equation (4.13), the in-phase and qradrature term of the virtual spacing can be obtained:

$$
V'_{I1} = V_{I1}V_{I2} - V_{Q1}V_{Q2} = \cos(k(d_1 + d_2)\sin\theta) = \cos(kd'_1 \sin\theta)
\tag{4.16}
$$

$$
V'_{Q1} = V_{Q1}V_{I2} + V_{I1}V_{Q2} = \sin(k(d_1 + d_2)\sin\theta) = \sin(kd'_1 \sin\theta)
\tag{4.17}
$$

$$
V'_{I2} = V_{I1}V_{I2} + V_{Q1}V_{Q2} = \cos(k(d_1 - d_2)\sin\theta) = \cos(kd'_2 \sin\theta)
\tag{4.18}
$$

$$
V'_{Q2} = V_{Q1}V_{I2} - V_{I1}V_{Q2} = \sin(k(d_1 - d_2)\sin\theta) = \sin(kd'_2 \sin\theta)
\tag{4.19}
$$

Now suppose that the chosen moduli set $[m_1\ m_2]$ is given by

$$
m_1 = hm_2
\tag{4.20}
$$

where h is the ratio of modulus m_1 and m_2.

From Equation (4.13) and Equation (4.14), using Equation (3.16),

$$d_1' = d_1 + d_2 = \frac{\lambda \hat{M}}{4N}\left(\frac{1}{m_1} + \frac{1}{m_2}\right)\xi = \frac{\lambda \hat{M}}{4N}\left(\frac{1+h}{m_1}\right)\xi = \frac{\lambda \hat{M}'}{4Nm_1'}\xi' \qquad (4.21)$$

$$d_2' = d_1 - d_2 = \frac{\lambda \hat{M}}{4N}\left(\frac{1}{m_1} - \frac{1}{m_2}\right)\xi = \frac{\lambda \hat{M}}{4N}\left(\frac{1-h}{m_1}\right)\xi = \frac{\lambda \hat{M}'}{4Nm_2'}\xi' \qquad (4.22)$$

This gives the relationship between a new moduli set $[m_1'\ m_2']$ with dynamic range $\hat{M}'$ and scale factor ξ'. Combining Equation (4.18) and Equation (4.19),

$$\left(\frac{1+h}{1-h}\right) = \frac{m_2'}{m_1'} \quad \longrightarrow \quad m_2' = m_1'\left(\frac{1+h}{1-h}\right) \qquad (4.23)$$

A suitable virtual moduli set $[m_1'\ m_2']$ can be found by using Equation (4.20) using the ratio h. A simple example illustrates how this virtual moduli set would work.

Consider a case of a two-channel RSNS interferometer using moduli set [8 16], the dynamic range for this set would be $\hat{M}=35$ and the scale factor $\xi = 1$. Let the frequency be 2.4 GHz ($\lambda = 12.5$ cm). The ratio,

$$h = \frac{m_1}{m_2} = \frac{8}{16} = \frac{1}{2}$$

The antenna spacings calculated from Equation (3.13) are

$$d_1 = \frac{\hat{M}\lambda}{4Nm_1} = \frac{35 \times 12.5}{4 \times 2 \times 8} = 6.8cm \qquad (4.24)$$

$$d_2 = \frac{\hat{M}\lambda}{4Nm_2} = \frac{35 \times 12.5}{4 \times 2 \times 16} = 3.4cm \qquad (4.25)$$

The resolution at broadside is given by Equation (3.20). For $AOA = 0°$ at broadside, the bin number, u, corresponds to 90.

$$r_{u=90} = \sin^{-1}\left(\frac{2u - \hat{M} + 2}{\hat{M}\xi}\right) - \sin^{-1}\left(\frac{2u - \hat{M}}{\hat{M}\xi}\right)$$

$$= \sin^{-1}\left(\frac{2(90) - 35 + 2}{35(1)}\right) - \sin^{-1}\left(\frac{2(90) - 35}{35(1)}\right) \qquad (4.26)$$

$$= 3.3°$$

From Equation (4.20),

$$m_2' = m_1'\left(\frac{1 + h}{1 - h}\right) = m_1'\left(\frac{1 + \frac{1}{2}}{1 - \frac{1}{2}}\right) = 3m_1' \qquad (4.27)$$

There could be several modular pairs which satisfy Equation (4.21) and Table 3 shows some of the possible pairs and their corresponding dynamic ranges.

m_1'	7	8	9	10
m_2'	21	24	27	30
$\hat{M}'$	45	51	57	63

Table 3.   Moduli sets and dynamic range for $h = \frac{1}{2}$ (From [6]).

Suppose that the chosen virtual moduli set is $[m_1'\ m_2'] = [10\ 30]$ with $\hat{M}' = 63$. The virtual scale factor can be found from Equation (4.18) or Equation (4.19),

$$d_1' = d_1 + d_2 = (6.8 + 3.4) = \frac{12.5(63)}{4(2)(10)}\xi' \qquad (4.28)$$

$$\xi' = 1.04$$

The resolution of the virtual moduli set is

$$r_{u=90}' = \sin^{-1}\left(\frac{2u - \hat{M}' + 2}{\hat{M}'\xi'}\right) - \sin^{-1}\left(\frac{2u - \hat{M}'}{\hat{M}'\xi'}\right)$$

$$= \sin^{-1}\left(\frac{2(90) - 63 + 2}{63(1.04)}\right) - \sin^{-1}\left(\frac{2(90) - 63}{63(1.04)}\right) \qquad (4.29)$$

$$= 1.8°$$

27

The virtual moduli set improved upon the resolution of the original array by almost 100%. In theory, super resolution could be achieved with a large number virtual moduli set $[m_1'\ m_2']$. However, the larger the m_1' or m_2', there would be a corresponding increase in the number of thresholds. As shown in Figure 8, these levels of threshold are closer together at the peaks and troughs of the folding waveform. Having the threshold levels closer can lead to quantization error in the presence of noise if the signal-to-noise ratio is low. It has been shown by Chen that in a low SNR environment, every moduli set would have regions where the transfer function "fades," i.e., where gross errors tend to occur [6].

C.   THREE-CHANNEL VIRTUAL SPACING INTERFEROMETRY

The virtual RSNS DF can be similarly extended to a *N*-channel system [3]. Let us consider a case of three-channel virtual DF array where the moduli set are related by

$$m_1 = hm_2 = h^2 m_3 \tag{4.30}$$

The ratio h must satisfy the condition $h \le \frac{1}{2}$ for three integer values of m_i to exist. Similar to the two-channel system, the virtual spacing may be extended to a three-channel system by defining d_3' as

$$d_3' = d_1 - d_2 - d_3 = \frac{\lambda \hat{M}}{4N}\left(\frac{1}{m_1} - \frac{1}{m_2} - \frac{1}{m_3}\right)\xi = \frac{\lambda \hat{M}}{4N}\left(\frac{1 - h - h^2}{m_1}\right)\xi = \frac{\lambda \hat{M}'}{4Nm_3'}\xi' \tag{4.31}$$

Rearranging Equation (4.18) with Equation (4.19) and Equation (4.30), we get

$$\left(\frac{1+h}{1-h}\right) = \frac{m_2'}{m_1'} \tag{4.32}$$

$$\left(\frac{1+h}{1-h-h^2}\right) = \frac{m_3'}{m_1'} \tag{4.33}$$

Depending on the ratio h, it is possible to select integer value of $[m_1'\ m_2'\ m_3']$ so as to form other virtual moduli sets. A simple algorithm can be implemented to post-process the AOA information using the virtual moduli set to increase the

resolution of the DF array. A simple algorithm flow with two levels of virtual resolution processing is shown in Figure 14.
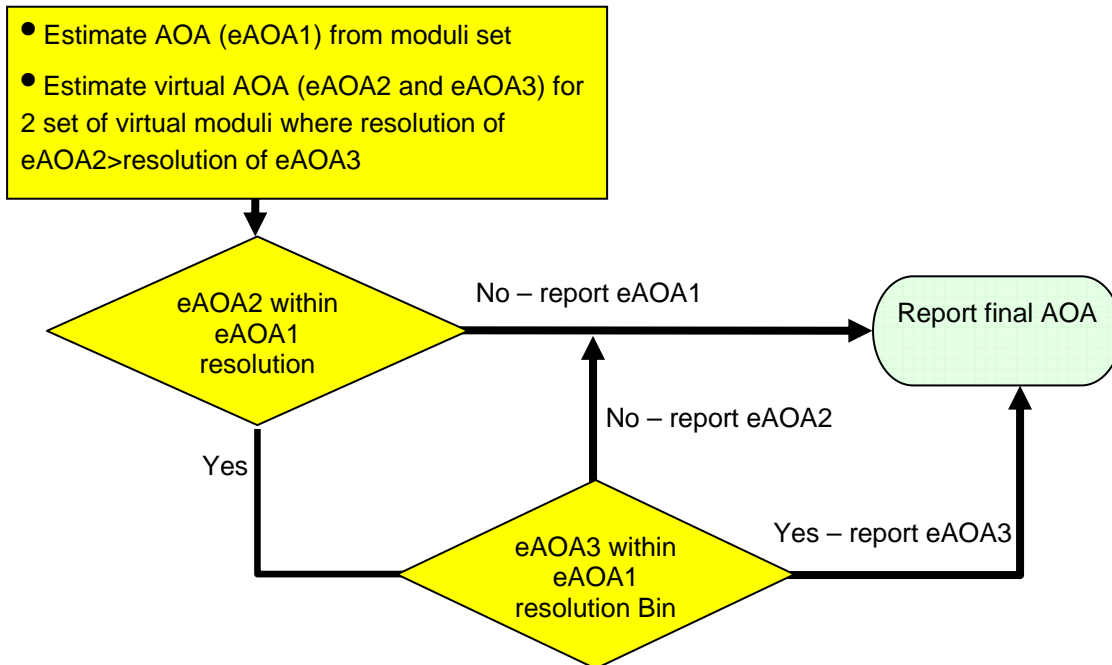
Figure 14.   Algorithm for two levels of virtual resolution processing (After [3]).

THIS PAGE INTENTIONALLY LEFT BLANK

V. DESIGN CONSIDERATIONS FOR THREE-CHANNEL RSNS VIRTUAL SPACING DIRECTION FINDING SYSTEM

This chapter presents some of the considerations in designing a three-channel RSNS virtual spacing DF system.

A. LIMITED REAL MODULI SET

Let $[m_1 \ m_2 \ m_3]$ be defined as the real moduli set where $m_1 < m_2 < m_3$. In order for virtual resolution to work, the real moduli set must satisfy Equation (4.27). Let the ratio, R, be defined as

$$R = \frac{h}{h^2} \tag{5.1}$$

As mentioned in the previous chapter, $h \leq \frac{1}{2}$ is required for three distinct positive integer values of the moduli set to exist. From Equation (5.1), $R \geq 2$ follows.

Based on these conditions, some of the possible real moduli sets which can be selected for a three-channel RSNS DF system are shown in Table 4 below.

	$[m_1 \ m_2 \ m_3]$	$\hat{M}$
	[2 4 8]	29
$h = \frac{1}{2}, \ R = 2$	[3 6 12]	41
	[4 8 16]	53
	[5 10 20]	65
	[2 6 18]	59
$h = \frac{1}{2}, \ R = 3$	[3 9 27]	86
	[4 12 36]	113
	[5 15 45]	140
	[2 8 32]	101
$h = \frac{1}{4}, \ R = 4$	[3 12 48]	149
	[4 16 64]	197
	[5 20 80]	245

Table 4.   Real moduli set $[m_1 \ m_2 \ m_3]$ and dynamic range for several values of h.

B.   LIMITED VIRTUAL MODULI SET

Let $[m'_1 \ m'_2 \ m'_3]$ be defined as the virtual moduli set where $m'_1 < m'_2 < m'_3$. For the virtual moduli set to have positive integer value, it needs to satisfy Equation (4.32) and Equation (4.33). Let the ratios, R_1 and R_2, be defined as

$$R_1 = \frac{m'_2}{m'_1} = \left(\frac{1+h}{1-h}\right) \tag{5.2}$$

$$R_2 = \frac{m'_3}{m'_1} = \left(\frac{1+h}{1-h-h^2}\right) \tag{5.3}$$

For the virtual moduli set to have positive integer value, m'_1 must satisfy both Equation (5.2) and Equation (5.3). Hence m'_1 has to be the multiple of lowest common denominator of R_1 and R_2. For $h = \frac{1}{2}$, $R_1 = 3$ and $R_2 = 6$. Since the lowest common denominator of R_1 and R_2 is 1, there is no restriction on the value of m'_1. For $h = \frac{1}{3}$, $R_1 = 2$ and $R_2 = \frac{12}{5}$. As the lowest common

denominator of R_1 and R_2 is 5, m_1' can be any multiple of 5. Table 5 lists some of possible the virtual moduli sets for selected ratios.

	$[\,m_1'\ m_2'\ m_3'\,]$	$\hat{M}'$
$h = \frac{1}{2}$ $R_1 = 2,\ R_2 = 6$	[2 6 12]	41
	[3 9 18]	59
	[4 12 24]	77
	[9 27 54]	167
$h = \frac{1}{3}$ $R_1 = 2,\ R_2 = \frac{12}{5}$	[5 10 12]	89
	[10 20 24]	179
	[15 30 36]	269
	[20 40 48]	359
$h = \frac{1}{4}$ $R_1 = \frac{5}{3},\ R_2 = \frac{20}{11}$	[33 55 60]	853
	[66 110 120]	1708
	[99 165 180]	2563
	[132 220 240]	3418

Table 5.   Virtual moduli sets $[\,m_1'\ m_2'\ m_3'\,]$ and dynamic range for several values of h.

C.   SENSITIVITY OF SIZE OF ANTENNA

The size of an antenna array is determined by Equation (3.16). If the design frequency f is fixed at 2.4 GHz, the antenna size is only dependent on the selection of modulus, m_i, dynamic range $\hat{M}$ and scale factor ξ. Since the dynamic range $\hat{M}$ is determined by modulus m_i, the antenna size is only dependent on two parameters, m_i and ξ.

The antenna spacing of the moduli set is listed in Table 6. It shows that the antenna array spacing is relatively insensitive to the selection of the real moduli set and more dependent on the ratio h.

	$[m_1\ m_2\ m_3]$	d_1 (cm)	d_2 (cm)	d_3 (cm)
$h = \frac{1}{2}$ $\xi = 1$	[2 4 8]	15.1	7.6	3.8
	[3 6 12]	14.2	7.1	3.6
	[4 8 16]	13.8	6.9	3.5
	[5 10 20]	13.5	6.8	3.4
$h = \frac{1}{3}$ $\xi = 1$	[2 6 18]	30.7	10.2	3.4
	[3 9 27]	29.9	10.0	3.3
	[4 12 36]	29.4	9.8	3.3
	[5 15 45]	29.2	9.7	3.2
$h = \frac{1}{4}$ $\xi = 1$	[2 8 32]	52.6	13.2	3.3
	[3 12 48]	51.7	12.9	3.2
	[4 16 64]	51.3	12.8	3.2
	[5 20 80]	51.0	12.8	3.2

Table 6.   Antenna spacing for $[m_1\ m_2\ m_3]$
(scale factor $\xi = 1$ and frequency at 2.4 GHz).

Changing the scale factor to $\xi = 1.154$ reduces the FOV to $\pm 60°$ but it increases the array spacing slightly as shown in Table 7.

	$[m_1\ m_2\ m_3]$	d_1 (cm)	d_2 (cm)	d_3 (cm)
$h = \frac{1}{2}$ $\xi = 1.154$	[2 4 8]	17.4	8.7	4.4
	[3 6 12]	16.4	8.2	4.1
	[4 8 16]	15.9	8.0	4.0
	[5 10 20]	15.6	7.8	3.9
$h = \frac{1}{3}$ $\xi = 1.154$	[2 6 18]	35.5	11.8	3.9
	[3 9 27]	34.5	11.5	3.8
	[4 12 36]	34.0	11.3	3.8
	[5 15 45]	33.7	11.2	3.7
$h = \frac{1}{4}$ $\xi = 1.154$	[2 8 32]	60.7	15.2	3.8
	[3 12 48]	59.7	14.9	3.7
	[4 16 64]	59.2	14.8	3.7
	[5 20 80]	58.9	14.7	3.7

Table 7.   Antenna spacing for $[m_1\ m_2\ m_3]$
(scale factor $\xi = 1.154$ and frequency at 2.4 GHz)..

D.   FIELD OF VIEW LIMITATION

The FOV of the real moduli set is determined by the Equation (3.15) while the FOV of the virtual moduli is determined by Equation (4.21), Equation (4.22) or Equation (4.31).   The critical parameter in determining the FOV is the ratio h. Table 8 and Table 9 list the FOVs of selected combinations of real and virtual moduli sets for $\xi = 1$ and $\xi = 1.154$.

	$[m_1\ m_2\ m_3]$	$[m'_1\ m'_2\ m'_3]$	FOV(deg)	FOV'(deg)
$h = \frac{1}{2}$ $\xi = 1$	[3 6 12]	[4 12 24]	±90	±69.9
		[9 27 54]	±90	±64.8
	[4 8 16]	[4 12 24]	±90	±75.6
		[9 27 54]	±90	±69.0
	[5 10 20]	[4 12 24]	±90	±80.8
		[9 27 54]	±90	±72.1
$h = \frac{1}{3}$ $\xi = 1$	[2 6 18]	[5 10 12]	±90	±26.9
		[10 20 24]	±90	±27.1
	[3 9 27]	[5 10 12]	±90	±27.8
		[10 20 24]	±90	±27.9
	[4 12 36]	[5 10 12]	±90	±28.2
		[10 20 24]	±90	±28.4
$h = \frac{1}{4}$ $\xi = 1$	[2 8 32]	[33 55 60]	±90	±24.2
		[66 110 120]	±90	±24.2
	[3 12 48]	[33 55 60]	±90	±24.6
		[66 110 120]	±90	±24.6
	[4 16 64]	[33 55 60]	±90	±24.8
		[66 110 120]	±90	±24.9

Table 8.   Field of view for selected moduli set, $\xi = 1$.

	$[m_1\ m_2\ m_3]$	$[m'_1\ m'_2\ m'_3]$	FOV(deg)	FOV'(deg)
	[3 6 12]	[4 12 24]	±60	±54.4
		[9 27 54]	±60	±51.6
$h = 1/2$	[4 8 16]	[4 12 24]	±60	±57.0
		[9 27 54]	±60	±54.0
$\xi = 1.154$	[5 10 20]	[4 12 24]	±60	±58.8
		[9 27 54]	±60	±55.5
	[2 6 18]	[5 10 12]	±60	±23.1
		[10 20 24]	±60	±23.2
$h = 1/3$	[3 9 27]	[5 10 12]	±60	±23.8
		[10 20 24]	±60	±23.9
$\xi = 1.154$	[4 12 36]	[5 10 12]	±60	±24.2
		[10 20 24]	±60	±24.3
	[2 8 32]	[33 55 60]	±60	±20.8
		[66 110 120]	±60	±20.8
$h = 1/4$	[3 12 48]	[33 55 60]	±60	±21.1
		[66 110 120]	±60	±21.2
$\xi = 1.154$	[4 16 64]	[33 55 60]	±60	±21.3
		[66 110 120]	±60	±21.3

Table 9.   Field of view for selected moduli set, $\xi = 1.154$.

The DF system's FOV is determined primarily by h and is relatively insensitive to the selection of the moduli set. As the ratio h decreases, the system's FOV reduces accordingly. For a given operational requirement of an instantaneous FOV, the choice of the ratio h could be limited.

E.   SELECTION OF MODULUS RATIO

Let the phase differences between every combination of element of a three-channel interferometer be defined as indicated in Figure 15. An ambiguity diagram can be used to determine which h ratio should be chosen. An ambiguity diagram is a phase-plane plot comparing the phase difference of an interferometer [14]. The closer the lines on the ambiguity diagrams, the poorer the interferometer will perform in determining the actual phase difference. To

further explain how the ambiguity diagram works, consider a simple three element interferometer with $d_1 = 3\left(\frac{\lambda}{2}\right)$ and $d_2 = 2\left(\frac{\lambda}{2}\right)$. The phase-plane plot of the corresponding ϕ_1 and ϕ_2 is given in Figure 16.
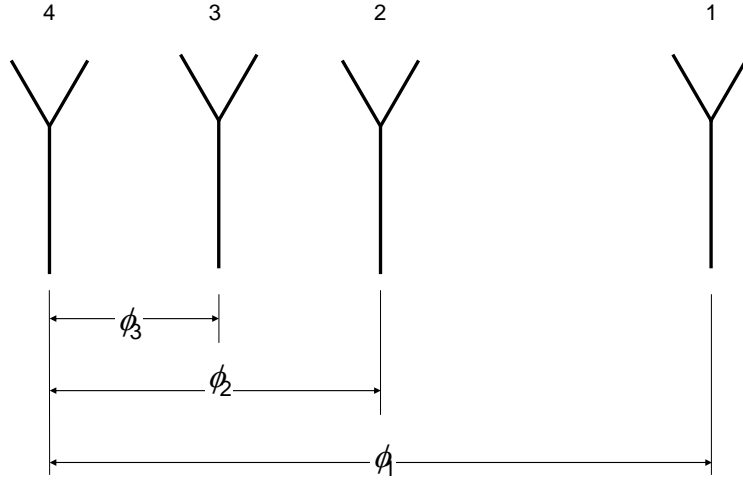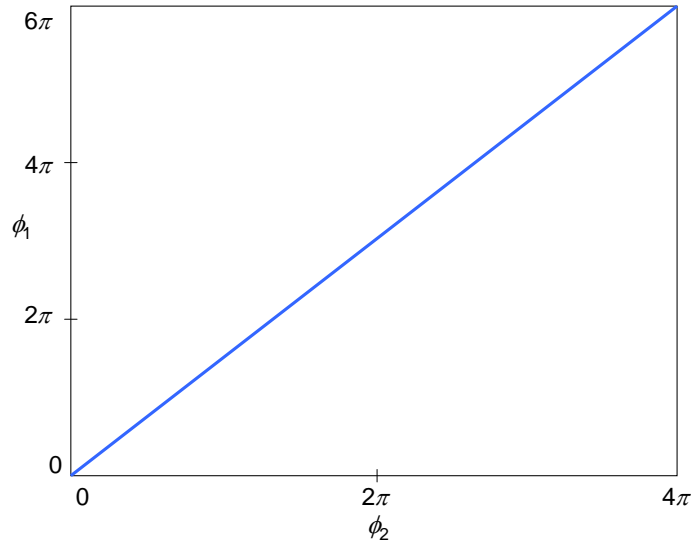

Figure 15.   Phase difference for a three-channel interferometer.

Figure 16.   Phase-plane plot for $d_1 = 3\left(\frac{\lambda}{2}\right)$ and $d_2 = 2\left(\frac{\lambda}{2}\right)$ (From [14]).

Since ϕ_1 and ϕ_2 can be known only to within 2π radian, Figure 16 can be normalized to 2π as shown in Figure 17. The ambiguity diagrams for selected ratios of $h = \frac{1}{2}$, $h = \frac{1}{3}$ and $h = \frac{1}{4}$ are given in Figures 18 to 20. These figures showed that the higher h ratio gives the best performance in resolving ambiguity between the phases as the lines are further apart.
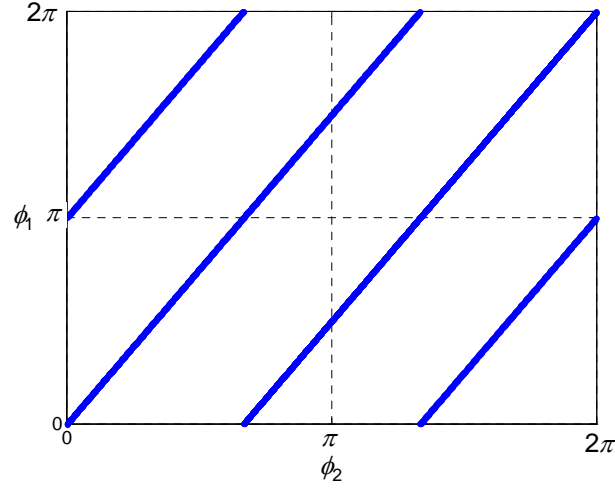

Figure 17.   Ambiguity diagram for $d_1 = 3\left(\frac{\lambda}{2}\right)$ and $d_2 = 2\left(\frac{\lambda}{2}\right)$ (From [14]).

In designing a RSNS virtual spacing DF system, it is important to select the highest possible h ratio. For any given h ratio and frequency, the size of the antenna array as well as the FOV of the system would not change significantly once the ratio has been selected The highest possible h ratio gives the best performance in resolving phase ambiguity.
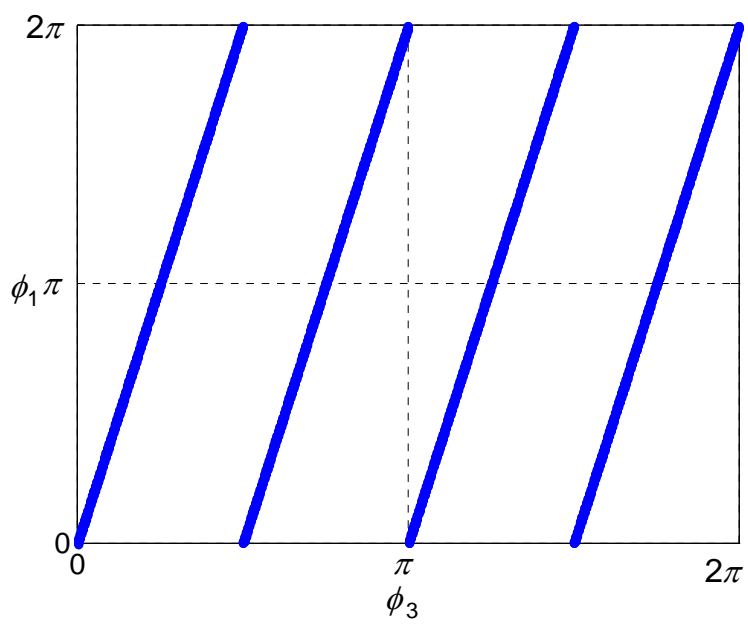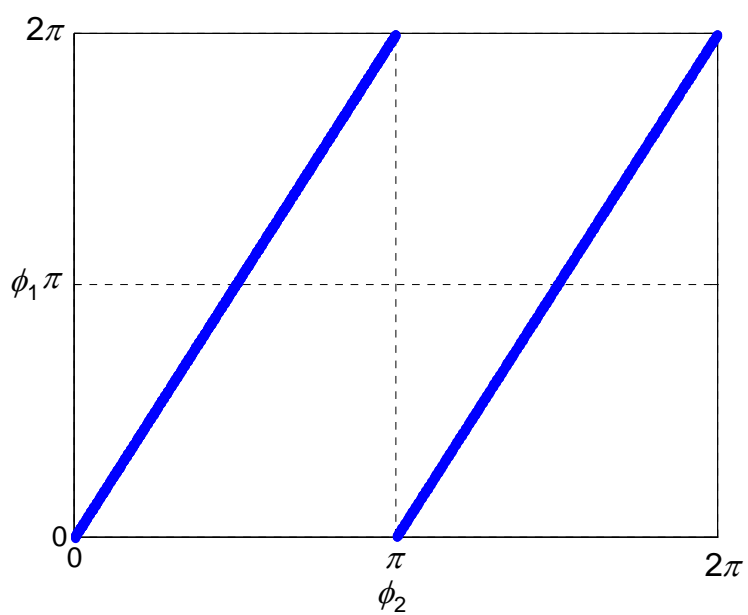
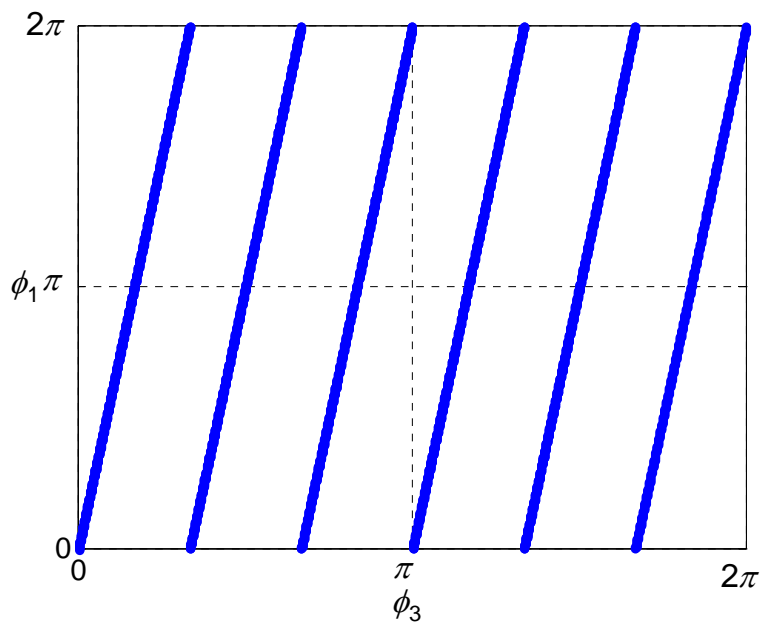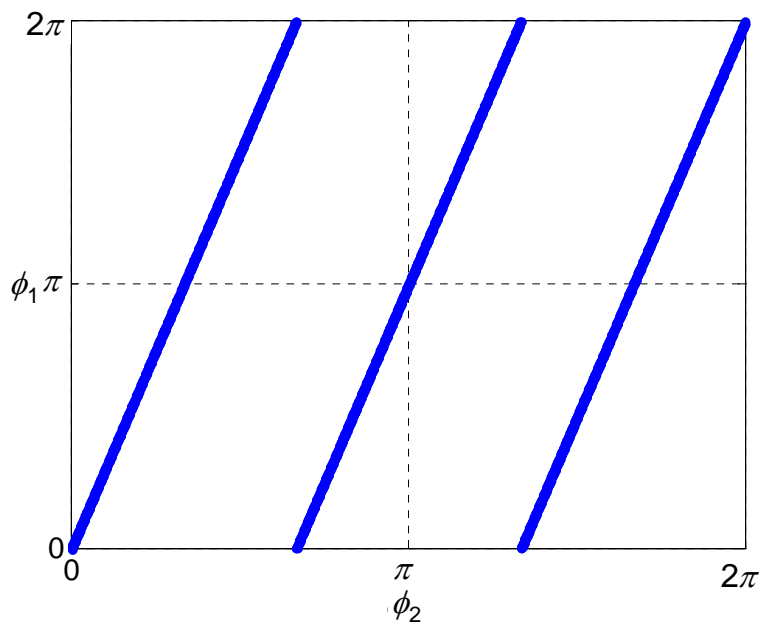Figure 18.   Ambiguity diagram for $h = \frac{1}{2}$.
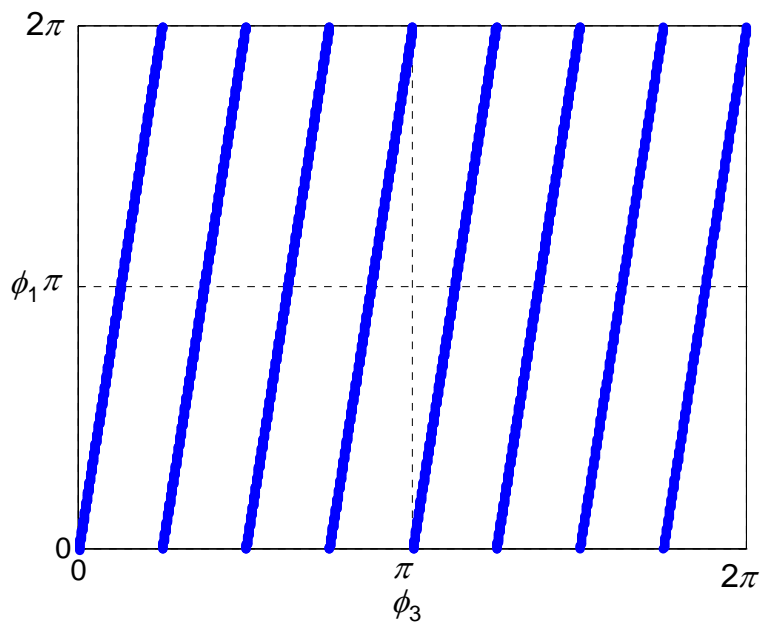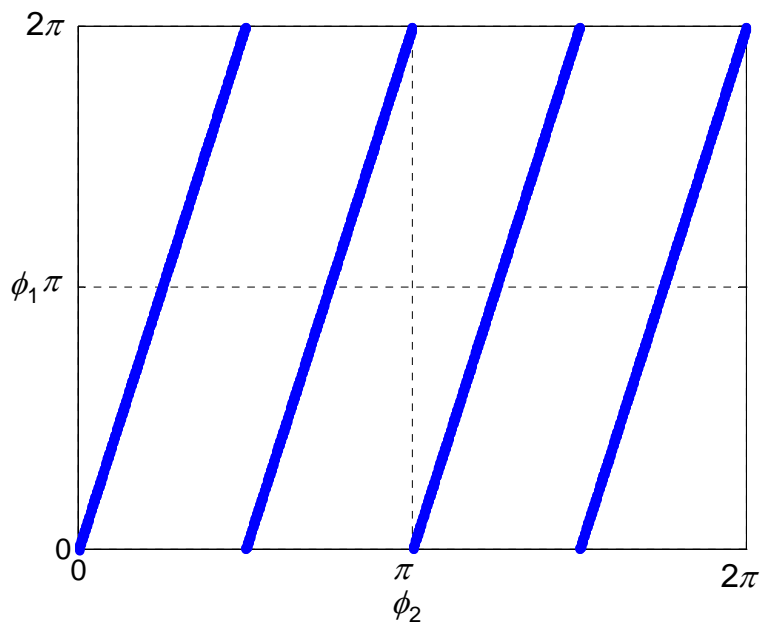
Figure 19. Ambiguity diagram for $h = \frac{1}{3}$.

Figure 20.   Ambiguity diagram for $h = \dfrac{1}{4}$.

THIS PAGE INTENTIONALLY LEFT BLANK

VI.   MODELING AND SIMULATION

To understand and predict the performance of a three-channel RSNS virtual spacing DF system, simulations in MATLAB were carried out. This chapter introduces all the models that were used in the MATLAB simulations.

A.   NOISE MODEL

It is assumed that the noise in the system is random in nature and Gaussian distributed. The bandpass Gaussian random noise signal can be represented by

$$W(t) = \text{Re}\left(\left|A(t)\right|e^{j\varphi(t)}e^{j\omega_c t}\right) \tag{6.1}$$

where

$\left|A(t)\right|$ is random process with Rayleigh first-order probability density function; and

$\varphi(t)$ - random process with uniform first-order probability over range $(0, 2\pi)$.

Using Euler's formula, Equation (6.1) can be written as:

$$W(t) = W_I \cos(\omega_c t) - W_Q(t) \sin(\omega_c t) \tag{6.2}$$

where

$$W_I(t) = \left|A(t)\right| \cos(\varphi(t)) \tag{6.3}$$
$$W_Q(t) = \left|A(t)\right| \sin(\varphi(t)) \tag{6.4}$$

From these equations and combining Equation (4.4) and Equation (4.5), the Gaussian noise model can be represented by

$$V_{I_{Noise}}(p_n, t) = V(p_n, t) + W_I(t) \tag{6.5}$$
$$V_{Q_{Noise}}(p_n, t) = V(p_n, t) + W_Q(t) \tag{6.6}$$

B. MONTE CARLO SIMULATION

Monte Carlo methods are commonly used in simulating physical or mathematical systems when a closed form statistical solution is too complex to resolve. It uses the Monte Carlo algorithm which can be easily implemented with a computer to model random processes. The Monte Carlo simulation is carried out to determine the performance of the three-channel RSNS virtual spacing DF system with random white Gaussian noise. First, a review of the Monte Carlo algorithm is given below [15].

Let a random variable X consist of both the signal voltage V together with random noise W, centered on zero with variance of one.

$$X = V + W \tag{6.7}$$

The probability of $X > z$ for any given V where z is constant is

$$P(z) = P\left(X > \frac{z}{V} \right) \tag{6.8}$$

By generating a series of statistically independent and identically distributed Gaussian random variable $w(n)$, where $n=1,2,…,N$ times, Equation (6.8) can be estimated. A new set of random variables, $x(n)$, can be found by adding a constant v to the $w(n)$.

$$x(n) = v + w(n) \tag{6.9}$$

Let a new random variable $y(n)$ be defined as

$$y(n) = \begin{cases} 0, & \text{if } x(n) \le z \\ 1, & \text{if } x(n) > z \end{cases} \tag{6.10}$$

The estimation of Equation (6.8) is

$$\hat{P}(z) = \frac{1}{N}\sum_{n=1}^{N} y(n) \tag{6.11}$$

The mean, $E\langle \bullet \rangle$, and variance, σ^2, of $\hat{P}(z)$ is

$$E\langle \hat{P}(z) \rangle = \frac{1}{N}\sum_{n=1}^{N} E\langle y(n) \rangle = \frac{1}{N}NP(z) = P(z) \tag{6.12}$$

$$\sigma_{\hat{P}(z)}^2 = E\langle\hat{P}(z) - P(z)\rangle = E\langle\hat{P}^2(z)\rangle - P^2(z) = \frac{1}{N}P(z)(1-P(z)) \qquad (6.13)$$

Let the required outcome probability of the estimation, α, be defined by

$$\alpha \leq P\left(\left|\hat{P}(z) - P(z)\right| < \varepsilon\right) \qquad (6.14)$$

where the relative error ε is defined as,

$$\varepsilon = \frac{\left|P(z) - \hat{P}(z)\right|}{P(z)} \qquad (6.15)$$

Using Chebyshev's inequality,

$$P\left(\left|\hat{P}(z) - P(z)\right| < \varepsilon\right) \geq 1 - \frac{\sigma_{\hat{P}(z)}^2}{\varepsilon^2} \geq \alpha \qquad (6.16)$$

Using Equation (6.13),

$$1 - \frac{\frac{1}{N}P(z)(1-P(z))}{\varepsilon^2} \geq \alpha$$

$$N \geq \frac{P(z)(1-P(z))}{(1-\alpha)\varepsilon^2} \qquad (6.17)$$

Equation (6.17) determines the number of times the simulation must be run to satisfy Equation (6.14) for any given α and ε. The Monte Carlo algorithm is summarized by the flowchart in Figure 21.
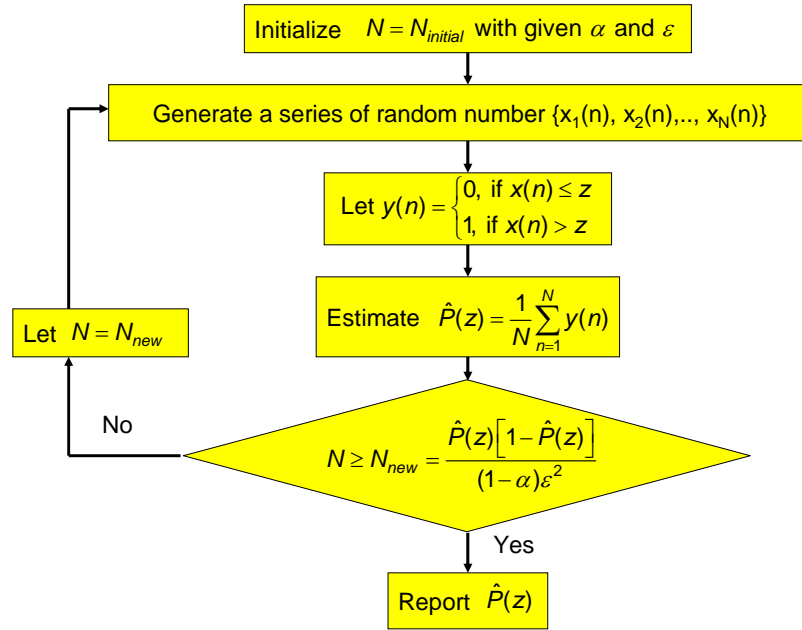
Figure 21. Monte Carlo algorithm.

C. HARDWARE SETUP

The simulations were based on the hardware used by Lee in his three-channel DF antenna array [3]. Figure 22 shows the block diagram of all the hardware used in the array.
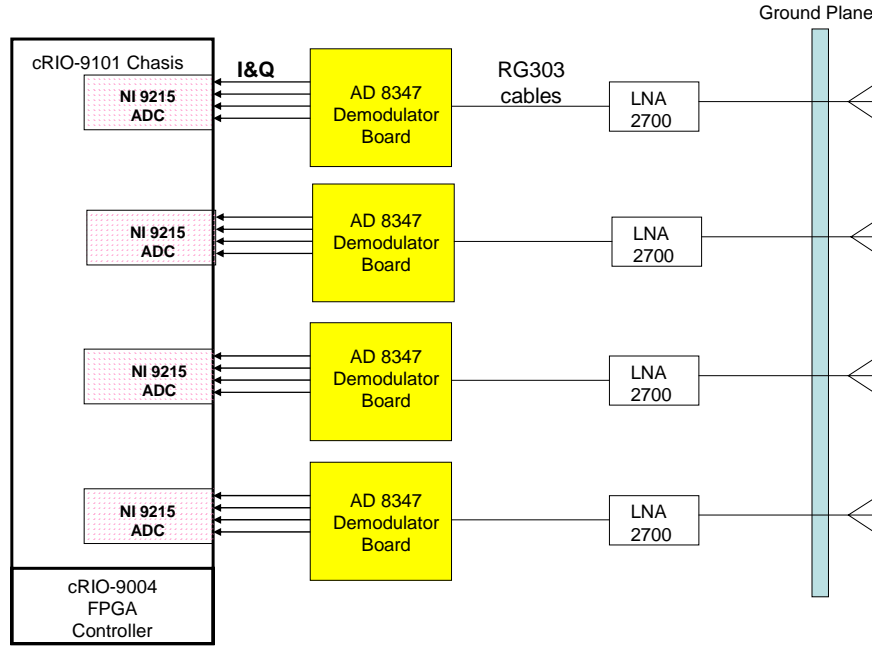
Figure 22.   Hardware block diagram of a three-channel DF antenna array.

To determine the SNR of the I and Q data after the demodulator board, a calculation of the noise figure was done for one receiver channel.   The specifications of the hardware used are given in Figure 23.
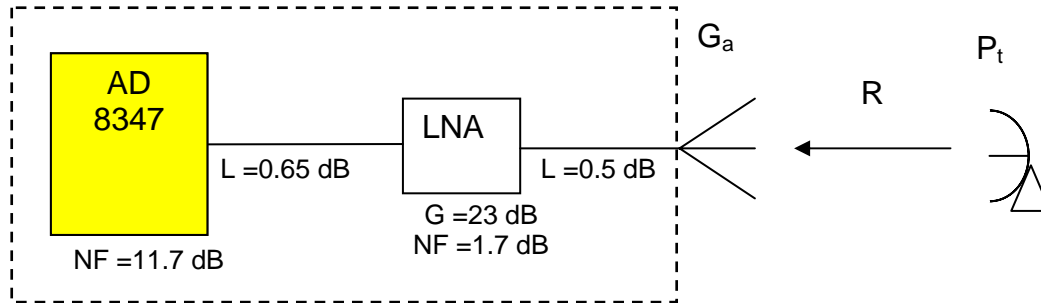

Figure 23.   Specifications for antenna array's noise figure.

The receiver's noise figure as shown in the dashed box is given by

$$F_e = F_1 + \frac{F_2 - 1}{G_1} + \frac{F_3 - 1}{G_1 G_2} + \frac{F_4 - 1}{G_1 G_2 G_3}$$ (6.18)

where

$F_1 = \frac{1}{G_1} = $ cable loss from antenna to LNA = 0.5 dB,

$F_2 = $ noise figure of LNA = 1.7 dB,

$G_2 = $ gain of LNA = 23 dB,

$F_3 = \frac{1}{G_3} = $ cable loss from LNA to AD 8347 demodulator = 0.65 dB,

$F_4 = $ noise figure of AD 8347 demodulator = 11.7 dB,

$G_4 = $ total gain of the demodulator baseband and RF amplifier.

From Equation (6.18),

$$F_e = 1.12 + \frac{1.48 - 1}{0.89} + \frac{1.16 - 1}{0.89 \times 199.5} + \frac{14.79 - 1}{0.89 \times 199.5 \times 0.86} \tag{6.19}$$

$$F_e = 1.77 \tag{6.20}$$

$$T_e = (F_e - 1)T_a = (1.77 - 1)290 = 223 \text{ K} \tag{6.21}$$

$$T_s = T_e + T_a = 223 + 300 = 523 \text{ K} \tag{6.22}$$

The noise power is

$$\begin{aligned} N_o &= k_B T_s B \\ &= 1.38 \times 10^{-23} \times 523 \times 50 \times 10^6 \\ &= 3.61 \times 10^{-13} \\ &= -124.4 \text{ dB} \end{aligned} \tag{6.23}$$

where B is the instantaneous receiver bandwidth (50 MHz). The minimum RF power that can be input to the AD 8347 depends on the sensitivity of the demodulator. From the specification, it ranges from -65 dBm to 0 dBm. Therefore the minimum power that the antenna dipole can receive is

$$P_{rec,min} = -65 + 0.65 - 23 + 0.5 - 6.55 = -93.4 \text{ dBm} \tag{6.24}$$

The minimum SNR output from the AD8347 demodulator board is

$$SNR_{min} = -93.4 - (-124.4) = 31.0 \text{ dB} \tag{6.25}$$

Assuming that atmospheric absorption is negligible, for any isotropic emitter transmitting an average power of P_t at distance R, the SNR can be determined by

48

$$SNR = \frac{P_t}{4\pi R^2 N_o} \tag{6.26}$$

Based on the calculated SNR, the variance of the noise is determined from

$$SNR = \frac{V_i^2}{2\sigma^2} \tag{6.27}$$

where V_i is the channel output voltage defined in Equation (4.16). For a one watt emitter, the maximum detection range of the current array is

$$SNR_{min} = \frac{P_t}{4\pi R_{max}^2 N_o} \tag{6.28}$$

$$1259 = \frac{1}{4\pi \times R_{max}^2 \times 3.61 \times 10^{-13}} \tag{6.29}$$

$$R_{max} = 13.2 \text{ km} \tag{6.30}$$

D.   ANTENNA PATTERN

The antenna array used by Lee utilizes vertical printed circuit dipoles and was designed for a nominal frequency of 2.4 GHz. It has been tested in the anechoic chamber by Burgstaller to determine the dipole antenna pattern [16]. Figure 24 shows the measured element patterns for a dipole antenna at 2.4 GHz.
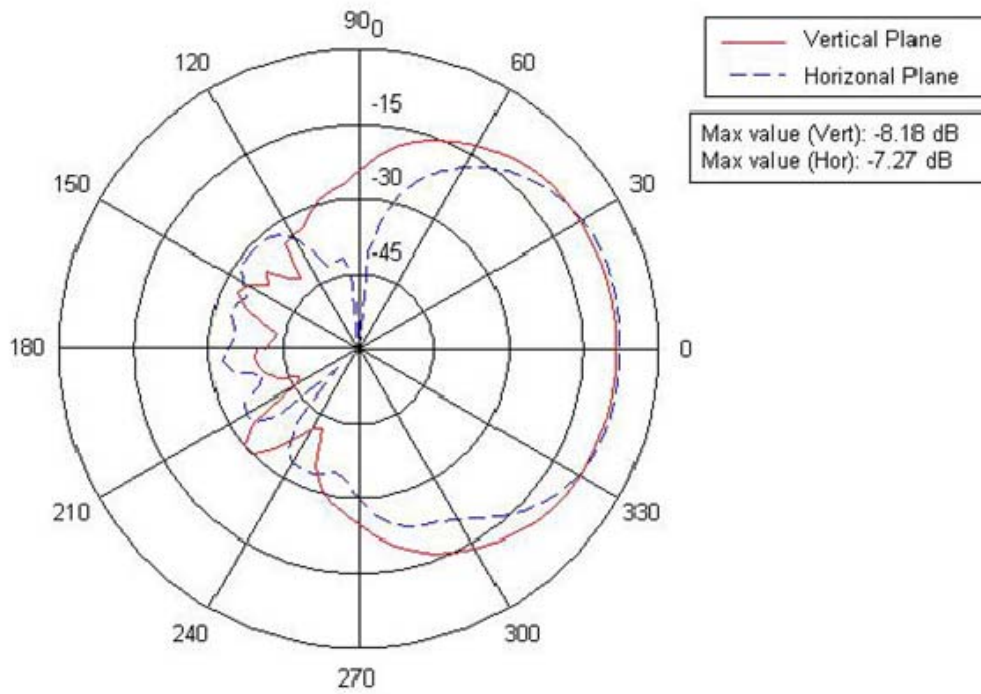
Figure 24.   Dipole element pattern measured at 2.4 GHz (From [13]).

The gain of the dipole element was measured to be 6.55 dB or 4.52 at broadside. The array estimates the AOA in the horizontal plane (H-plane). For the simulation, a simple cosine model was used to replicate the antenna pattern for various AOA

$$G_a = 4.52 \times \cos(\theta) \tag{6.31}$$

All the tools used in the simulation have been presented and the next chapter presents the results from simulations that were carried out.

VII. RESULTS AND ANALYSIS

With all the tools of the simulation in place, a sensitivity analysis was carried out to find out how some of these errors might affect the performance of the RSNS-based DF system.

A. BASELINE DESIGN PARAMETER

A three-channel RSNS virtual spacing DF design was chosen as a baseline design before any sensitivity analysis could be carried out. Using the steps described in Chapter III, the design parameters for a three-channel RSNS virtual DF system were chosen. It was decided that the design would be based on the hardware shown in Figure 22; hence the design frequency of 2.4 GHz was selected.

1. Determine *N*, the number of channels required.

A three-channel DF system was to be designed. Hence, *N*=3 and a total of four antenna elements would be required.

2. Identify an integer valued modulus for each channel (m_1, m_2 m_3).

Before identifying the moduli sets, the ratio *h* must first be selected. The three-channel RSNS virtual spacing DF system in Lee's thesis was based on $h = \frac{1}{2}$. The size of the antenna array built was about 14 cm. Experiment results shown that a number of gross errors appeared throughout the transfer function. Although the sources of errors were not fully investigated by Lee, it was suspected that the errors were due to mutual couplings as the antenna spacing between the antenna elements was small. It was decided that $h = \frac{1}{3}$ would be appropriate to reduce the effects from mutual couplings as well as to obtain a reasonable system's FOV.

Based on $h = \frac{1}{3}$, the real moduli set of [2 6 18] was selected so as to reduce quantization error when noise is present. The virtual moduli sets of [5 10 12] and [15 30 36] were selected to enable the DF system to have sufficient resolution.

3. **Determine the system dynamic range, $\hat{M}$, based on the chosen moduli.**

   From Table 4 and Table 5, the dynamic ranges for the all the moduli sets are listed in Table 10.

Moduli set	Dynamic Range
[2 6 18]	$\hat{M}_{Real} = 59$
[5 10 12]	$\hat{M}'_{Virtual1} = 89$
[15 30 36]	$\hat{M}'_{Virtual2} = 269$

Table 10. Dynamic ranges for baseline design.

4. **Determine the numbers of folds, n_i, for each modulus.**

   The numbers of folds are given in Table 11.

Moduli Set	Number of folds
[2 6 18]	$n_1 = 4.92$ $n_2 = 1.64$ $n_3 = 0.55$
[5 10 12]	$n_1' = 2.97$ $n_2' = 1.48$ $n_3' = 1.24$
[15 30 36]	$n_1' = 2.99$ $n_2' = 1.49$ $n_3' = 1.25$

Table 11.   Numbers of folds for baseline design.

5.   **Determine the required antenna spacing, d_i, for each channel.**

The required antenna spacing for all moduli sets are given below in Table 12.

Moduli Set	Antenna spacing
[2 6 18]	$d_1 = 30.73$ cm $d_2 = 10.24$ cm $d_3 = 3.41$ cm
[5 10 12]	$d_1' = 39.33$ cm $d_2' = 19.67$ cm $d_3' = 16.39$ cm
[15 30 36]	$d_1' = 39.33$ cm $d_2' = 19.67$ cm $d_3' = 16.39$ cm

Table 12.   Antenna spacing for baseline design.

6. Re-mapping the Field of View (FOV).

The real moduli set's FOV was not scaled and hence the scale factor $\xi_{real} = 1$. The FOV of the three-channel system is given in Table 13.

Moduli set	Scaling Factor	FOV (degree)
[2 6 18]	1	±90
[5 10 12]	2.21	±26.9
[15 30 36]	2.19	±27.1

Table 13.   Scale factor and FOV for baseline design.

7. Determine the thresholds.

The threshold levels for all the moduli sets are shown graphically in Figure 25-27.
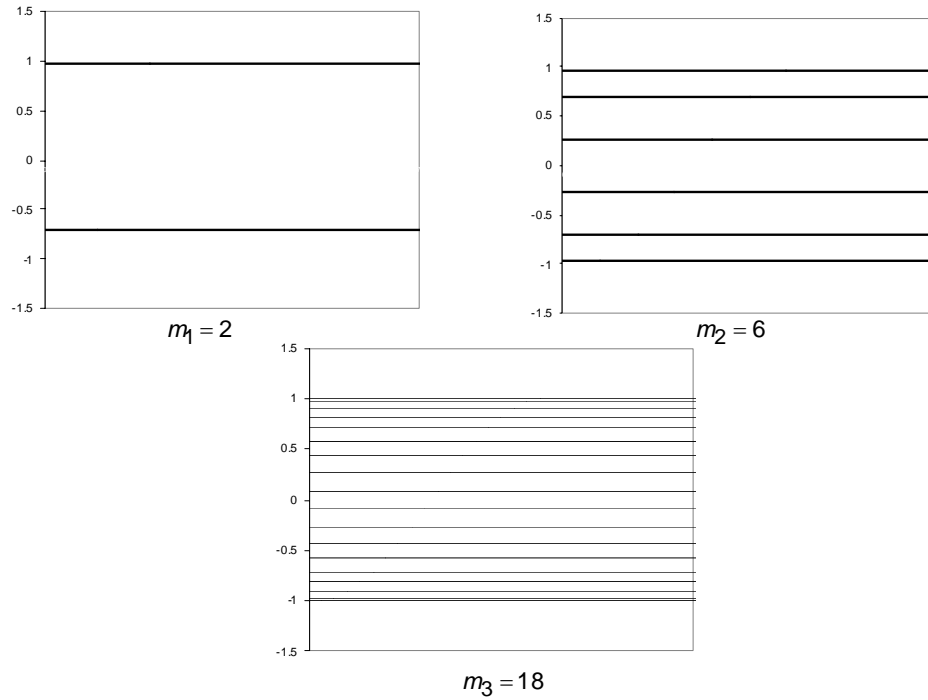

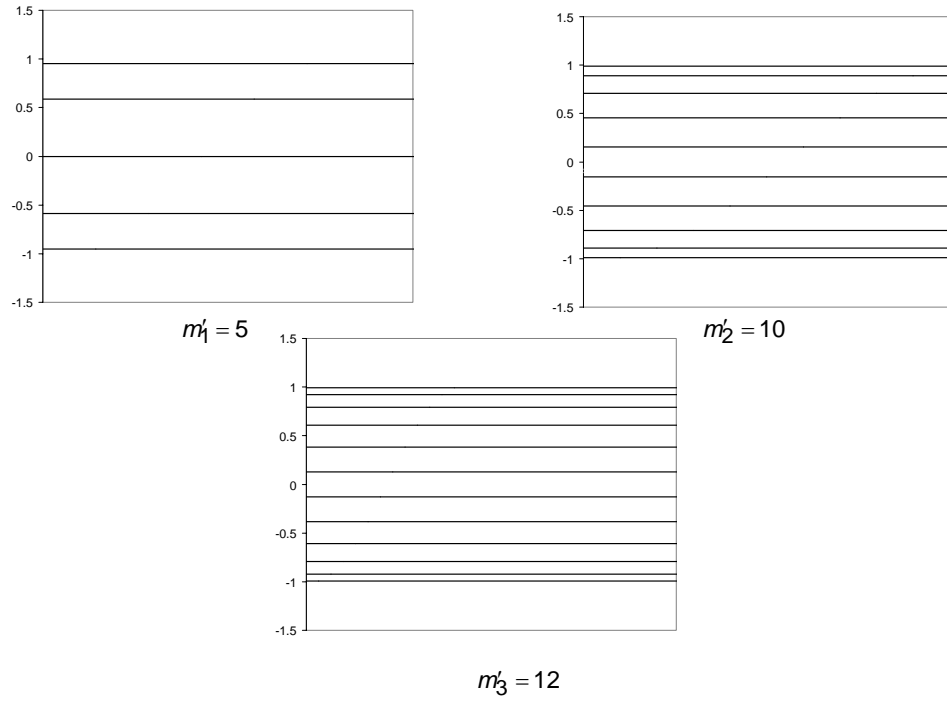Figure 25.   Threshold levels for real moduli set [2 6 18].

$m_1' = 5$

$m_2' = 10$

$m_3' = 12$

Figure 26.   Threshold levels for first virtual moduli set [5 10 12].
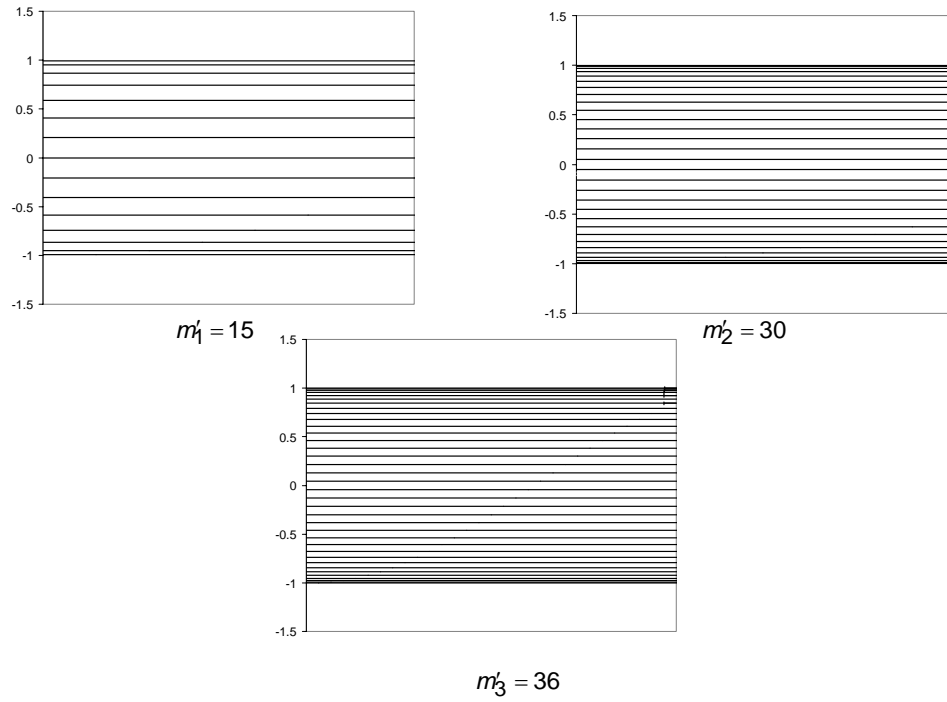

$m_1' = 15$

$m_2' = 30$

$m_3' = 36$

Figure 27.   Threshold levels for second virtual moduli set [15 30 36].

8.   Calculate the phase adjustment term, ζ_i, for each channel.

The phase adjustment terms, ζ_i, for the moduli sets are listed in Table 14.

Moduli set	Phase Adjustment term, ζ
[2 6 18]	$\zeta_1 = 2.36$ $\zeta_2 = -1.48$ $\zeta_3 = 1.54$
[5 10 12]	$\zeta_1' = -0.94$ $\zeta_2' = -2.15$ $\zeta_3' = 1.79$
[15 30 36]	$\zeta_1' = -1.15$ $\zeta_2' = -2.18$ $\zeta_3' = 1.82$

Table 14.   Phase adjustment term for baseline design.

The ideal transfer function for the baseline design is given in Figure 28. The baseline design has a broadside resolution of **0.19 deg RMS**. In practice, it is not possible to achieve this accuracy as there would be errors which have not been accounted for in the current baseline design. A one watt emitter at a detection range of 12 km for the current hardware is used as a scenario. This scenario gives a SNR of approximately 38 dB. Using this scenario and with the addition of Gaussian noise as described in Chapter VI, the transfer function is given in Figure 29. The RMS error is approximately **0.5 deg RMS.**
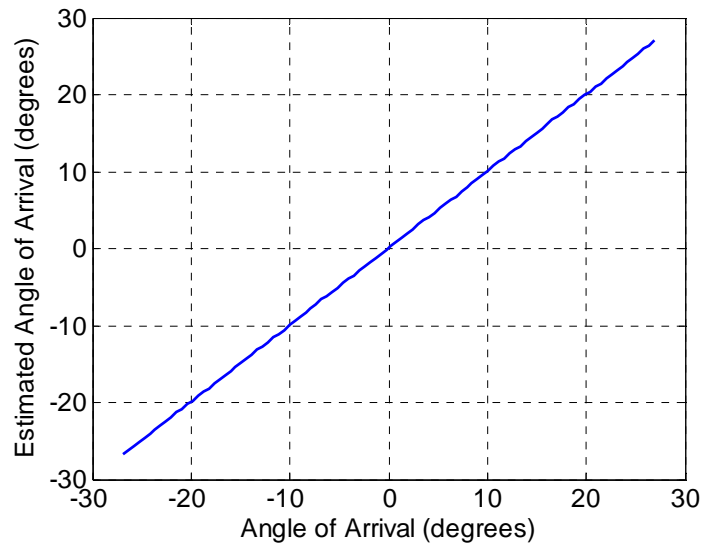
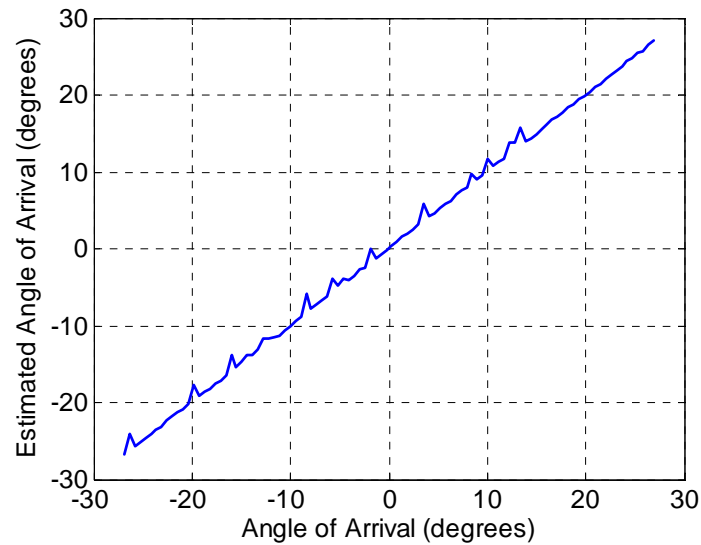Figure 28.   Transfer function for the baseline design.

Figure 29.   Transfer function with noise.

The transfer function shown in Figure 29 represents a snapshot of the transfer function in time.   Over time, the transfer function would vary due to random noise. In order to figure out how the noise would affect the probability of estimating the correct AOA over time, a Monte Carlo simulation was carried out. For the Monte Carlo simulation, the following parameters were used:

Relative error, $\varepsilon = 3\%$.

Required outcome probability , $\alpha = 90\%$.

For the given scenario, there is a greater than 50% probability that the correct AOA will be estimated within the FOV as shown in Figure 30. In order to satisfy Equation (6.14), the number of times the simulation needs to be run is 2777. In practice, 2777 readings would need to be taken from the emitter when the determining the AOA for the results of the Monte Carlo simulation to hold true. As this is not realistc, a comparison between the probabilities of taking a reduced sample size of 100 readings against 2777 readings is given in Figure 31. It shows that a reduced sample of 100 readings has good correlation to the full Monte Carlo simulation results. Therefore, even if a reduced sample size of 100 readings is used, the results from the Monte Carlo simulation would still hold true.
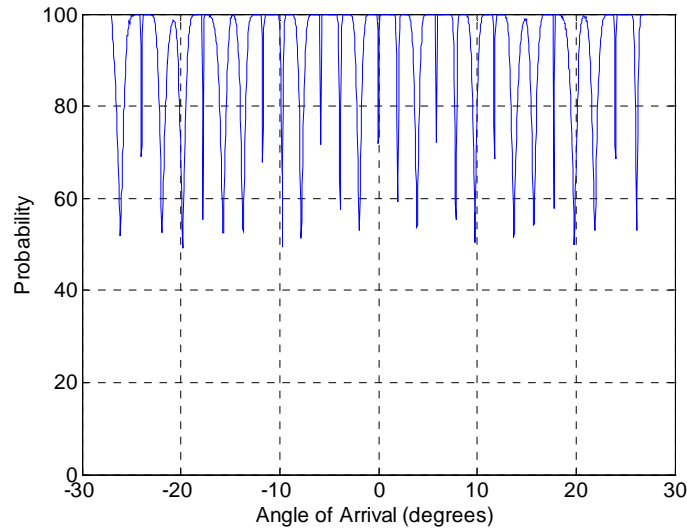

Figure 30.   Probability of correct AOA estimation for
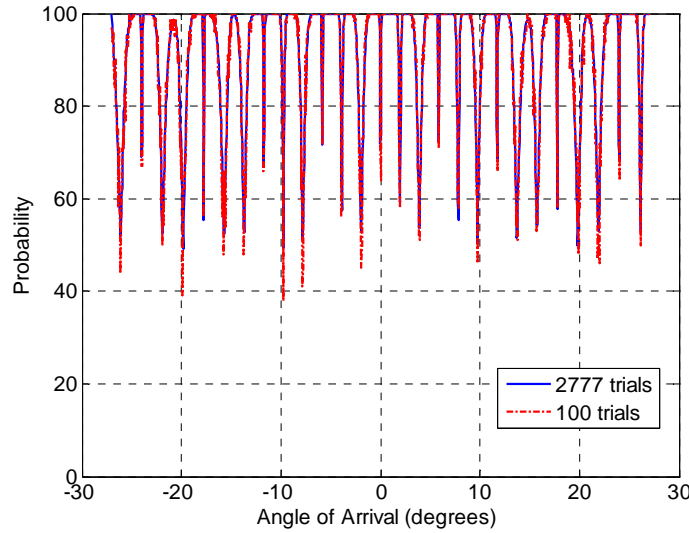baseline design.

Figure 31. Probability of correct AOA estimation for
full sample size vs 100 sample size.

B. EFFECTS OF SPACING ERROR

As it is unlikely that the array would be precisely constructed, the effects of spacing error were investigated. By adding a manufacturing error of 2 mm and 4 mm along the array axis into the element spacing, the transfer functions were plotted in Figure 32. The spacing error does not affect the transfer function significantly for spacing errors of 2 mm while spacing errors of 4 mm introduce more fading regions away from the broadside. These spacing errors correspond to 0.016 and 0.032 wavelength displacements in the horizontal direction. Note that position errors along the array axis do not affect AOA estimate near the broadside. Position errors out of the array plane will affect the AOA estimates near the broadside.
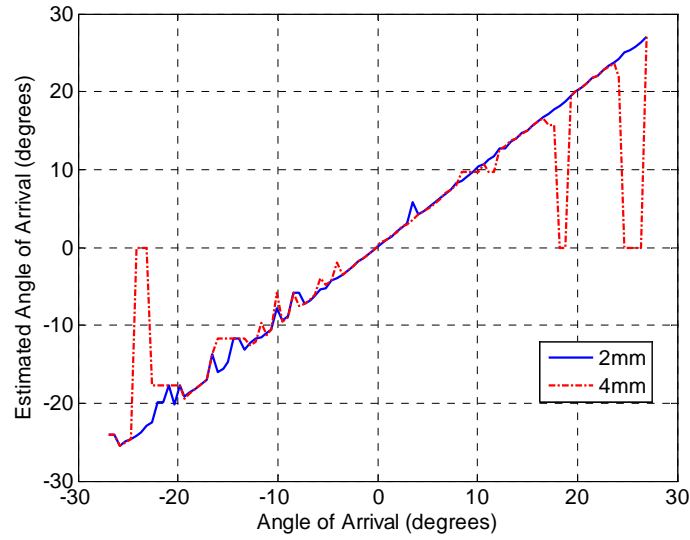
Figure 32.   Transfer function with noise and spacing errors.

The probability of correct AOA estimation for spacing errors of 2 mm and 4 mm is given in Figure 33. Comparing Figure 30 and Figure 33, spacing errors do not affect the probability of correct AOA estimation. These results suggest that small spacing error does not have significant effect on the performance of the RSNS virtual spacing DF system.
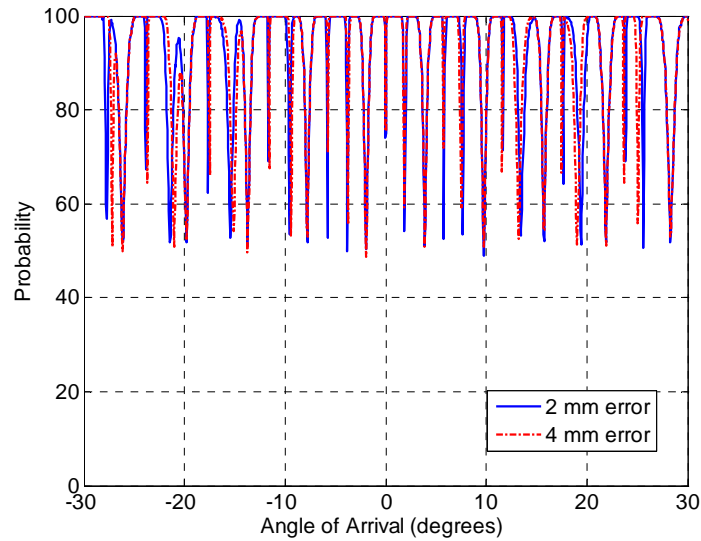

Figure 33.   Probability of correct AOA estimation with spacing errors.

C. EFFECTS OF PHASE ERROR

There may be residual phase errors introduced into the DF system that may not be possible to remove during the calibration. Such phase errors could result from a different antenna temperature and cable phase error. By adding a phase error of 5 degrees and 10 degrees to all the channels, the transfer function is plotted in Figure 34. Comparing Figure 29 with Figure 34 shows that the phase error affected the transfer function accuracy significantly. As the phase error increases, the transfer function has more fading regions.
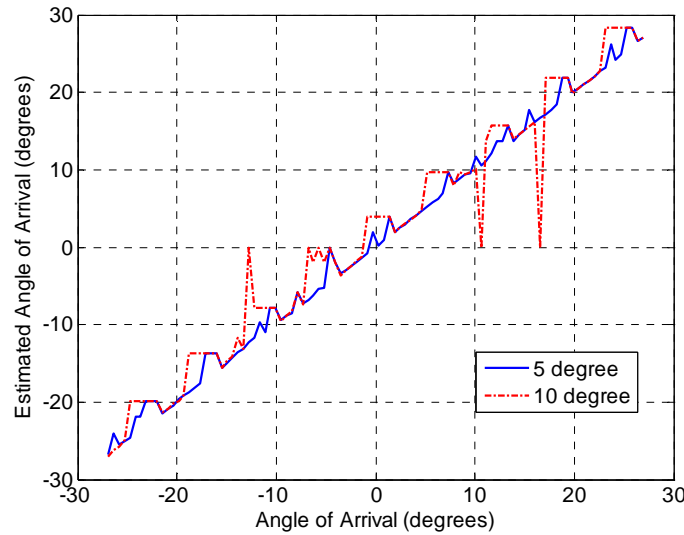

Figure 34. Transfer function with noise and phase errors.

The probability of correct AOA estimation with phase errors is plotted in Figure 35. It showed with phase error the probability of correct AOA estimation reduces and increasing the phase error further reduces the probability. These results indicated that phase errors need to be minimized as much as possible during the hardware design as well as during DF system operation to improve the accuracy of the DF system.
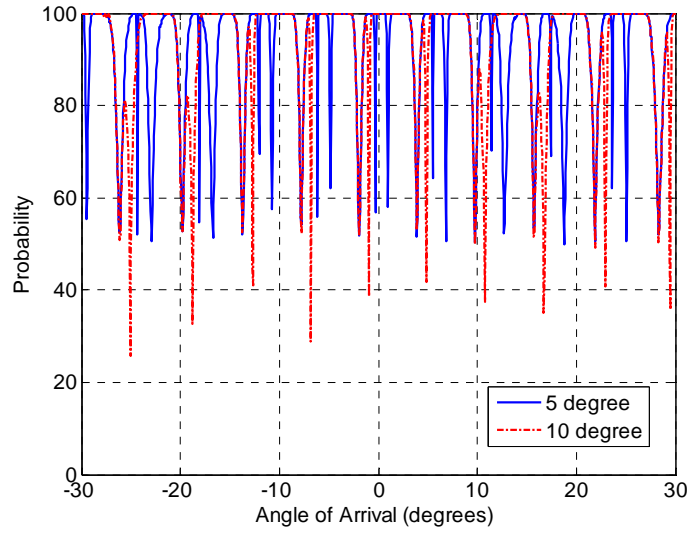
Figure 35.   Probability of correct AOA estimation with phase errors.

D.   EFFECTS OF FREQUENCY CHANGE

In all the previous simulations, it was assumed that the frequency of the signal was fixed at 2.4 GHz.   In order to investigate into how sensitive the baseline design was to changes in the frequency, the physical spacing of the antenna elements was fixed at d_1=30.93 cm, d_2=10.44 cm and d_3=3.61 cm. The signal frequency was varied to investigate its effect on the performance of the baseline design.   It was observed in Figure 36 that tolerance up to ±200 MHz bandwidth is possible without affecting the accuracy of the transfer function. As the signal frequency deviates away from the design frequency, the corresponding transfer function also deviates accordingly. This can be seen in Figure 37 where the slope of the transfer function for a 2.0 GHz signal no longer resembles the slope of the transfer function for a 2.4 GHz signal. The change in slope is predictable and can be compensated in the processing.
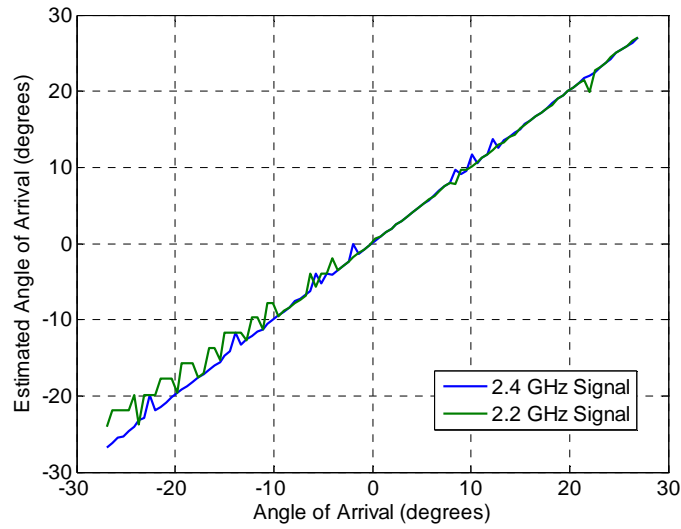
Figure 36.   Transfer function with noise using 2.4 GHz and 2.2 GHz signal.
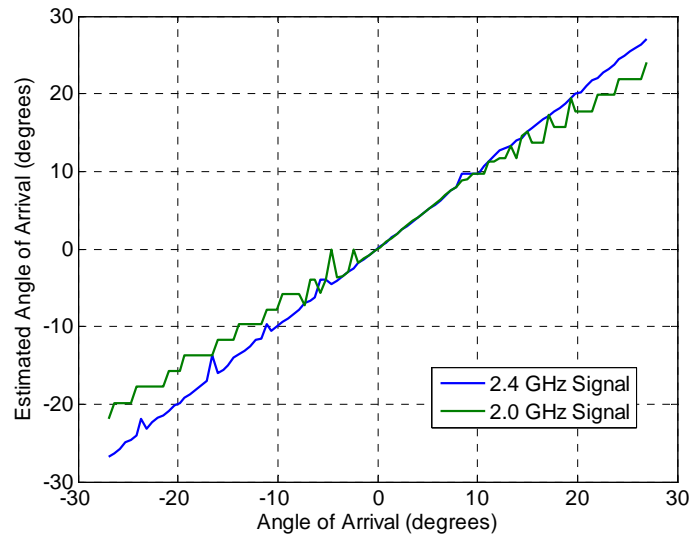

Figure 37.   Transfer function with noise using 2.4 GHz and 2.0 GHz signal.

As Figure 38 shows, there is no change in the probability of correct AOA estimation even with a 2.0 GHz signal. To design for a wideband frequency RSNS DF array would require several antenna baselines to cover the desired bandwidth with the necessary accuracy.
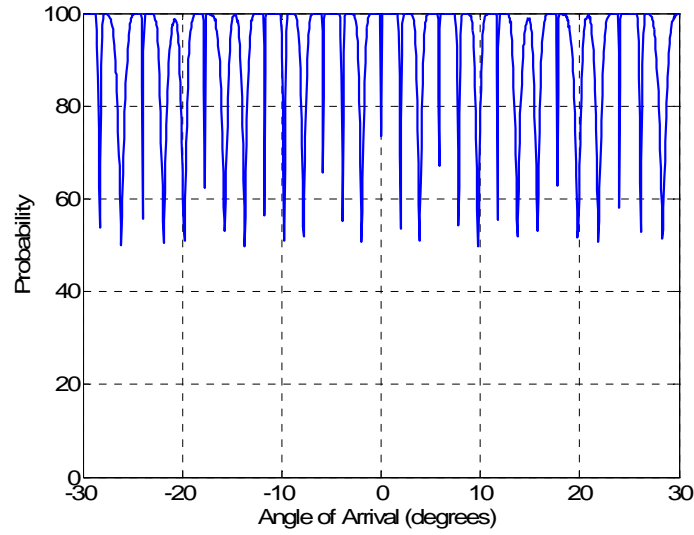
Figure 38.   Probability of correct AOA estimation baseline design
with 2.0 GHz signal.

E.   ALTERNATE MODULI SET

The baseline design's low value moduli set was selected after taking into consideration quantization errors in a low SNR scenario. The drawback of such a low moduli set was a small dynamic range, which resulted in lower resolution. To understand the effect of moduli change, an alternate higher moduli set was chosen for comparison while keeping the same *h* ratio. Table 15 shows the alternate moduli set and some of the key parameters obtained.

Moduli set	Dynamic Range	Antenna spacing	FOV (degree)
[4 12 36]	$\hat{M}_{Real} = 113$	$d_1 = 29.43$ cm $d_2 = 9.81$ cm $d_3 = 3.27$ cm	± 90
[10 20 24]	$\hat{M}'_{Virtual1} = 179$	$d'_1 = 39.24$ cm $d'_2 = 19.62$ cm $d'_3 = 16.35$ cm	± 28.4
[20 40 48]	$\hat{M}'_{Virtual2} = 359$	$d'_1 = 39.24$ cm $d'_2 = 19.62$ cm $d'_3 = 16.35$ cm	± 28.5

Table 15.   Alternate moduli set's parameters.

The alternate moduli set has an error of approximately **0.09 deg RMS** against the previous baseline design error of 0.5 deg RMS. The increase in accuracy was due to the higher dynamic range of the new moduli set. Using a similar scenario, the transfer function and the probability was plotted in Figure 39 and Figure 40. During multiple simulation runs, the occurrence of gross error was observed more often than the baseline design. This observation showed up in the resulting lower probability for correct AOA estimation in Figure 40. While the higher moduli set increases resolution, it trades off on the overall probability of correctly predicting the AOA.
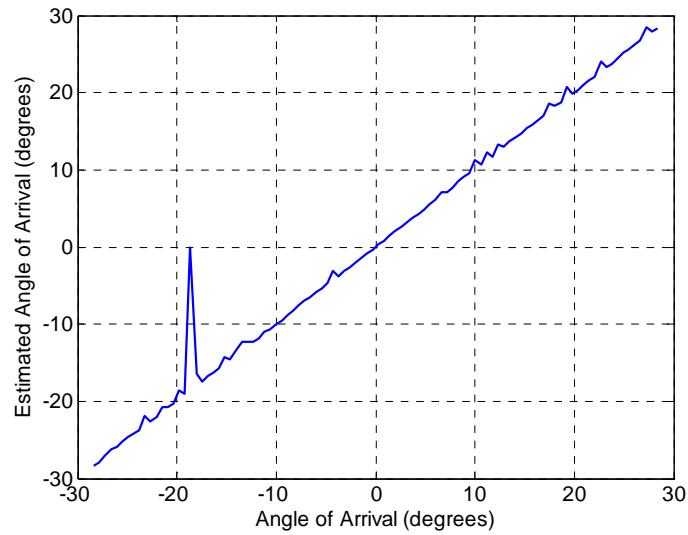
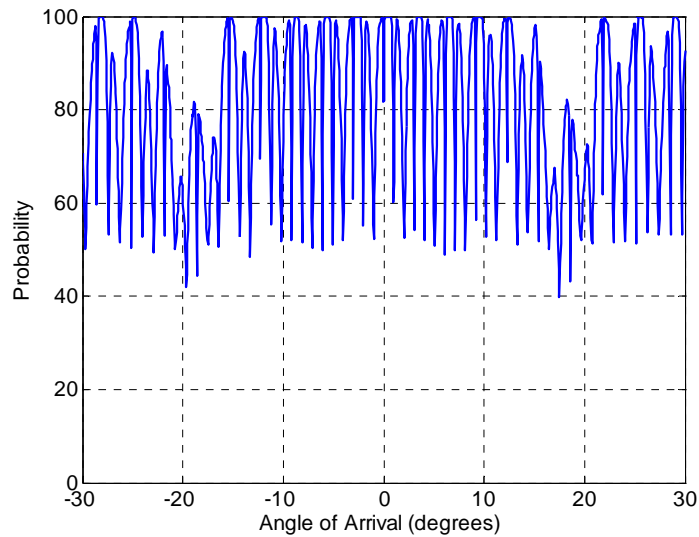Figure 39.   Transfer function of alternate moduli set.

Figure 40.   Probability of correct AOA estimation for alternate moduli set.

The effects of spacing errors and phase errors were also plotted for the alternate moduli set in Figure 41 and Figure 42. The tolerance to spacing error increased but the tolerance to phase error decreased. Using a 2.0 GHz signal, the alternate moduli set exhibits the similar effects of frequency changes as the baseline design. This can be seen in Figure 43.
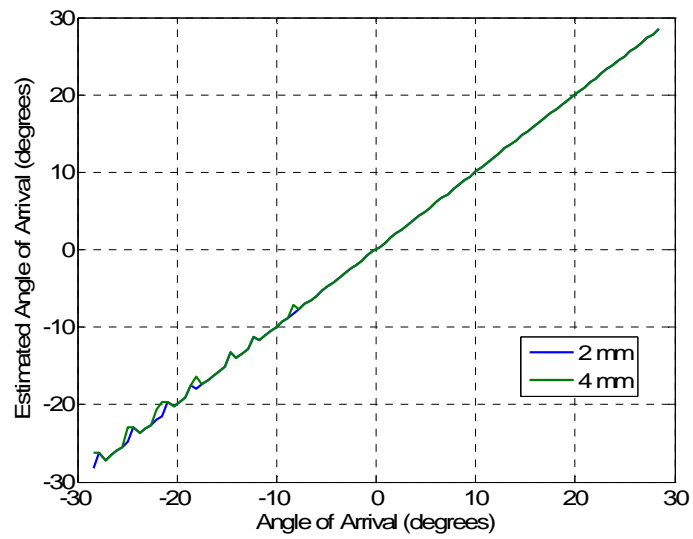
66

Figure 41. Transfer function for alternate moduli with spacing errors.
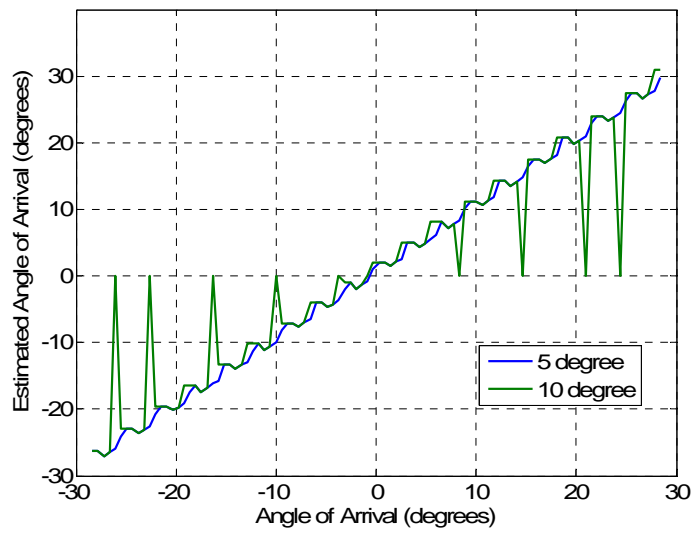

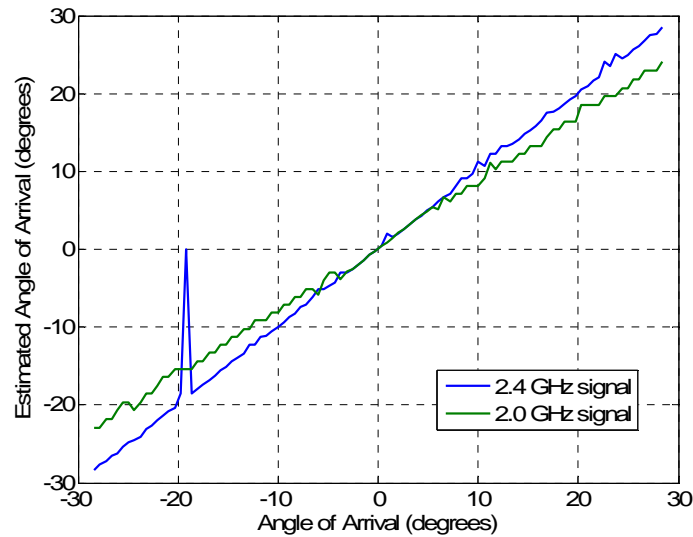Figure 42. Transfer function for alternate moduli with phase errors.

Figure 43.   Transfer function for alternate moduli using 2.4 GHz
and 2.0 GHz signal.

F.   EFFECTS OF SNR CHANGE

If the demodulator board is replaced with another of higher sensitivity, the baseline design would be able to handle a much lower SNR. This would enable the RSNS virtual DF system to increase its maximum range of detection. To investigate the effects of such low SNR, a one watt emitter is simulated at 30 km and 60 km. The probability of correct AOA estimation was plotted for both the baseline design and the alternate moduli set design. While both designs showed a reduction in probability, the alternate moduli set's performance at longer range, which translates to low SNR, was inferior to the baseline design. This can be clearly seen by comparing Figure 44 and Figure 45 for a signal at 60 km. The probability of correct AOA estimation for the baseline design was more than 50% while it was less than 50% for the alternate moduli set.

In order to select the correct moduli set, the most probable SNR condition needs to be assessed. If a low SNR condition is expected, the baseline design could be used. If a high SNR condition is expected, the alternate moduli set should be used instead.

68

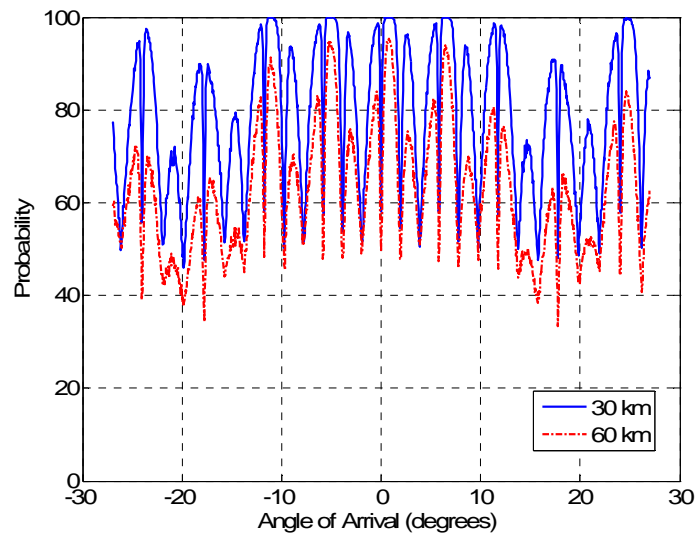Figure 44.   Probability of correct AOA estimation for baseline design with emitter at various ranges.
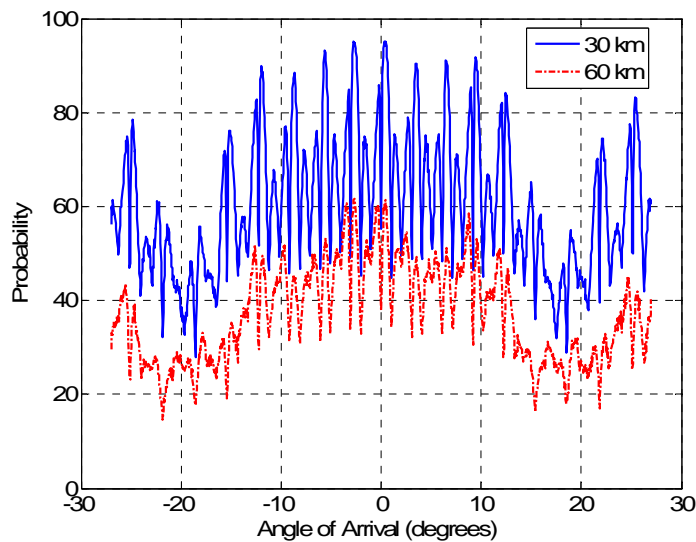

Figure 45.   Probability of correct AOA estimation for alternate moduli with emitter at various ranges.

G.   USING TWO SET OF MODULI

Since the RSNS-based interferometer was relatively insensitive to small spacing error, an investigation into using two complete sets of different moduli

based on the same ratio was carried out. Based on the ratio, $h = \frac{1}{3}$, the baseline moduli set and alternate moduli set was selected. Using the baseline design's spacing distance, the alternate moduli set was used together with the baseline moduli set. Although this effectively introduced spacing error into the alternate moduli set, the limited impact on the accuracy of the transfer function may be worth the tradeoff for higher probability of correct estimation in low SNR conditions. The transfer function for the baseline and alternate moduli set is shown in Figure 46.
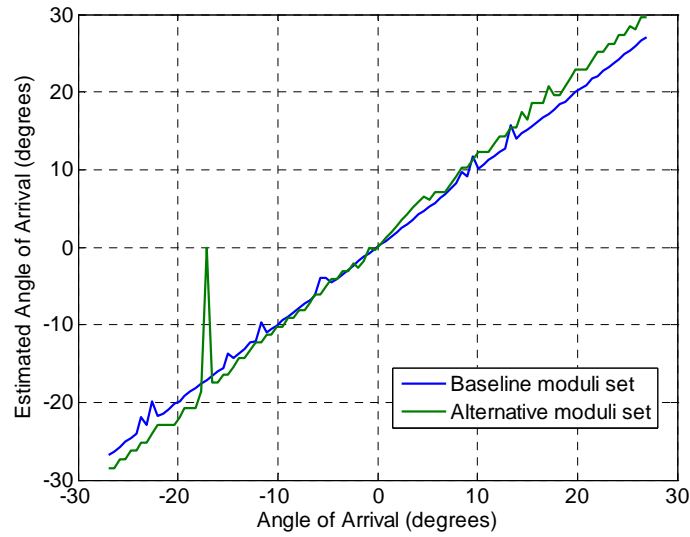

Figure 46.   Transfer function for baseline and alternate modui set.

VIII. CONCLUSION

This thesis focused on the design and analysis of a three-channel RSNS virtual spacing DF system. By analyzing a chosen design with addition of Gaussian noise as well as carrying out Monte Carlo simulations, the sensitivities to spacing error, phase error, frequency error, moduli set change and SNR change were determined. The baseline design showed good tolerance to most of these errors and should be considered for situations where low SNR is expected. For situations where high SNR is expected, the alternate moduli set should be selected. As the RSNS-based DF system was robust to the small spacing error, the best solution could be the dual use of both low and high moduli set. This would give a high probability of correct estimation at all time while retaining the accuracy of correcting mapping of the estimated AOA to the actual AOA.

The application of RSNS virtual spacing to DF has been demonstrated both theoretically as well as experimentally in the past. It showed great promise in applying this concept to platforms that have limited size but yet require high accuracy for DF. From a military perspective, an unmanned aerial vehicle used to detect a low probability of intercept emitters is one of the likely scenarios where RSNS-based DF concept could be applied.

Some of the possible future research areas to continue this RSNS-based DF concept are:

1. To build the baseline design using available hardware and verify the performance of the design with its theoretical performance. With the experimental data, other errors could be identified and corrected. Initial testing could be done in the laboratory before expanding it to field testing.

2. To determine the best set of two or more moduli set in order to optimize the performance of the RSNS-based DF system.

3.	Further improvement of the simulation by including the effects of mutual coupling interference.

4.	The use of non-PRP moduli set resulted in a smaller dynamic range than what would have been possible with a PRP moduli set. Studies into the use of PRP moduli set for virtual spacing should continue in order to fully exploit the advantage RSNS-based DF system.

LIST OF REFERENCES

[1]   Hendon H. Jenkins, *Small-Aperture Radio-Direction Finding,* pp 1, 11-18, Artech House, Norwood, Masachusetts, 1991.

[2]   Stephen E. Lipsky, *Microwave Passive Direction Finding,* pp 8-9, 155-166, John Wiley & Sons, New York, 1987.

[3]   Anthony Lee, "Variable Resolution Direction Finding using the Robust Symmetrical Number system," Master's Thesis, Naval Postgraduate School, Monterey, California, December 2006.

[4]   D. Wickersham, "Application of the Robust Symmetrical Number System to High Resolution Direction Finding Interferometry," Master's Thesis, Naval Postgraduate School, Monterey, California, 2000.

[5]   N. York, "Design of a Phase Sampled Interferometry Antenna Using the Robust Symmetrical Number System," Master's Thesis, Naval Postgraduate School, Monterey, California, 2000.

[6]   J.C. Chen, "A Virtual RSNS Direction Finding Antenna System," Master's Thesis, Naval Postgraduate School, Monterey, California, December 2004.

[7]   C.F.Babb, "Mixed Signal Processor for a Robust Symmetrical Number System Direction Finding Antenna," Master's Thesis, Naval Postgraduate School, Monterey, California, 2000.

[8]   P. E. Pace, D. Wickersham, D. Jenn, and N.York, "High Resolution Phase Sampled Interferometry Using Symmetrical Number Systems," *IEEE Transactions on Antennas and Propagation,* Vol. 49, No. 10, pp. 1411-1423, 2001.

[9]   I.A. Akin, "A Robust Symmetrical Number System with Gray Code Properties for applications in Signal Processing," Master's Thesis, Naval Postgraduate School, Monterey, California, 1997.

[10]   D. Styer and P.E. Pace, "Two-channel RSNS Dynamic Range," *IEEE Transactions on Circuits and Systems - I: Fundamental Theory and Applications*, Vol. 49, No.3, pp 395-397, 2002.

73

[11] P. E. Pace, D. Styer and I. A. Akin, "A folding ADC preprocessing architecture employing a robust symmetrical number system with Gray-code properties," *IEEE Trans. on Circuits and Systems-II: Analog and Digital Signal Processing,* Vol. 47, No. 5, pp. 462-467, 2000.

[12] Brian L. Luke, "Architecture of an Integrated Microelectronic Warfare System on a Chip and Design of Key Components," PhD Dissertation, Naval Postgraduate School, Monterey, California, 2004.

13] Brian L. Luke, P. E. Pace, "*N*-Sequence RSNS Ambiguity Analysis," *IEEE Trans. on Information Theory,* Vol. 53, No. 5, pp. 1759-1766, 2007.

[14] Goodwin, Robert L, "Ambiguity-Resistant Three- and Four-Channel Interferometers," NRL Report 8005, Naval Research Laboratory, Washington, D.C., September 1976.

[15] Peyton Z. Peebles, Jr., *Probability, Random Variables And Random Signal Principles,* pp 164-167, McGraw-Hill, New York, 2001.

[16] Burgstaller, G., "Wirelessly Networked Digital Phased Array: Design and Analysis of a 2.4GHz Demonstrator," Master's Thesis, Naval Postgraduate School, Monterey, California, September 2006.

INITIAL DISTRIBUTION LIST

1.   Defense Technical Information Center
      Ft. Belvoir, Virginia

2.   Dudley Knox Library
      Naval Postgraduate School
      Monterey, California

3.   Chairman, Code PH
      Naval Postgraduate School
      Monterey, California

4.   Prof. Phillip E. Pace
      Department of Electrical & Computer Engineering
      Naval Postgraduate School
      Monterey, California

5.   Prof. David C. Jenn
      Department of Electrical & Computer Engineering
      Naval Postgraduate School
      Monterey, California

6.   Prof. Donald L. Walters
      Department of Physics
      Naval Postgraduate School
      Monterey, California

7.   Bill Bigas
      EDO/ RSS
      Morgan Hill, California

8.   Dr. Jerry Fudge
      L-3 Communication
      Integrated Systems
      Greenville, TX

9.   Kevin Kwai
      Republic of Singapore Airforce
      Singapore